H2 Guaranteed Cost Control in Track-Following Servos

Richard Conway, Jianbin Nie, and Roberto Horowitz

Computer Mechanics Laboratory

Mechanical Engineering

University of California, Berkeley, CA, USA

December 29, 2011

Abstract

This chapter presents two new control synthesis approaches for dual-stage track-following servo systems. Both approaches are based on $\mathcal{H}_2$ guaranteed cost analysis, in which an upper bound on the worst-case $\mathcal{H}_2$ performance of a discrete-time system with gain-bounded unstructured causal LTI uncertainty is determined by solving either a semi-definite program (SDP) or several Riccati equations. We review the results of a paper on $\mathcal{H}_2$ guaranteed cost analysis and a paper on optimal full information $\mathcal{H}_2$ guaranteed cost control and then use these results to develop two output feedback control synthesis approaches. The first approach is based entirely on the solution of SDPs whereas the second approach exploits Riccati equation structure to reduce the number and complexity of the SDPs that need to be solved. Throughout the paper, we apply the analysis and control techniques to a hard disk drive model with a PZT-actuated suspension and demonstrate that the approaches that exploit Riccati equation structure are faster and at least as accurate as their SDP counterparts.

1
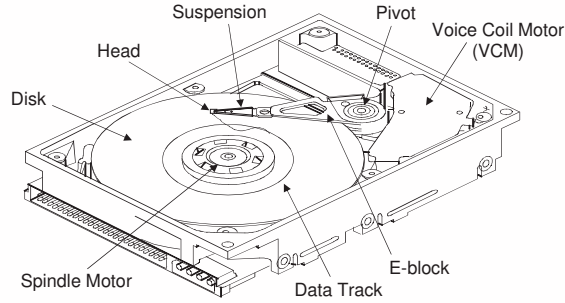
Figure 1: Schematic of a typical HDD

1   Introduction

For several decades now, the areal storage density of hard disk drives (HDDs) has been doubling roughly every 18 months, in accordance with Kryder's law. As the storage density is pushed higher, the concentric tracks on the disk which contain data must be pushed closer together, which requires much more accurate control of the read/write head. Currently available hard drives can store 2 TB of data on a 3.5" drive with three platters. This corresponds to an areal data density of 600 gigsbits/in^2. The current goal of the magnetic recording industry is to achieve an areal storage density of 4 terabits/in^2. It is expected that the track width required to achieve this data density is 25 nm. To achieve this specification for track-following control, in which the read/write head is maintained as close to the center of a given data track as possible, the 3σ value of the closed-loop position error signal (PES) should be less than 2.5 nm.

To help achieve this goal, the use of a secondary actuator has been proposed to give increased precision in read/write head positioning. There are three classes of secondary actuators: actuated suspensions [6], actuated sliders [7], and actuated heads [17]. Each of these proposed secondary actuator classes correspond to a different actuator location in Fig. 1. In the actuated head configuration, a microactuator (MA) actuates the read/write head with respect to the slider mounted at the tip of the suspension. In the actuated slider configuration, an MA directly actuates the head/slider assembly with respect to the suspension. For both of these configurations, it is difficult to design an MA which can be easily incorporated into the manufacture and assembly of a HDD on a large scale. In the actuated suspension configuration, the MA actuates the suspension with respect to the E-block. This secondary actuator scheme is the least difficult to design and has been incorporated into some consumer products. We will use this secondary actuation scheme in this paper.

Since there tend to be large variations in HDD dynamics due to variations in manufacture and assembly, it is not enough to achieve the desired level of performance for a single plant; the controller must guarantee the desired level of performance for a large set of HDDs. Thus, we are interested in finding a controller which

gives robust performance over a set of HDDs. One framework for solving this problem is guaranteed cost control. This methodology is a control design methodology whose objectives involve worst-case quadratic time domain costs over a modeled set of parametric uncertainty. Both the state feedback synthesis problem and the output feedback synthesis problem can be solved for discrete-time systems by using semi-definite programs (SDPs)—convex optimization involving linear matrix inequalities (LMIs)—as is done in [14] and [18], respectively.

As mentioned earlier, the relevant performance metric in a HDD is the standard deviation of the PES. Since the squared $\mathcal{H}_2$ norm of a system can be interpreted as the sum of variances of the system outputs under the assumption that the system is driven by independent white zero mean Gaussian signals with unit covariance, the $\mathcal{H}_2$ norm is a useful performance metric for HDDs.

This chapter reviews the basic results of $\mathcal{H}_2$ guaranteed cost analysis [3], which use the techniques of guaranteed cost control to yield an upper bound on the worst-case $\mathcal{H}_2$ performance of a system with dynamic unstructured uncertainty. Using this characterization of performance, we then review the solution of the corresponding full information control problem [4]—a generalization of the state feedback control problem—and use the results to generate two heuristics for solving the output feedback control problem.

For all of the problems in this chapter, we consider two approaches: an approach based on solving SDPs and an approach based on solving Riccati equations. Parallel to reviewing and developing the relevant theory, we apply these techniques to the design and analysis of HDD track-following controllers. For all numerical experiments in this paper, we use a 2.2 GHz Intel Core 2 Duo processor with 2 GB RAM running MATLAB 7.4.0 (with multithreaded computation disabled) under 32-bit Windows Vista. We solve SDPs two ways in this paper: using SeDuMi [16] with YALMIP [12] and using the `mincx` command in the Robust Control Toolbox for MATLAB without YALMIP. Through these HDD track-following control examples, we demonstrate the computational advantages of the approach based on Riccati equation solutions.

1.1 Preliminaries

In this chapter, we will denote the spectral norm (i.e. the maximum singular value) and the Frobenius norm of a matrix M respectively as $\|M\|$ and $\|M\|_F$. We will say that M is Schur if all of its eigenvalues lie strictly inside the unit disk in the complex plane. The operator "diag" takes several matrices and stacks them diagonally:

$$\text{diag}[M_1, \ldots, M_n] = \begin{bmatrix} M_1 & & 0 \\ & \ddots & \\ 0 & & M_n \end{bmatrix}. \tag{1}$$

(a) Lower LFT (b) Upper LFT
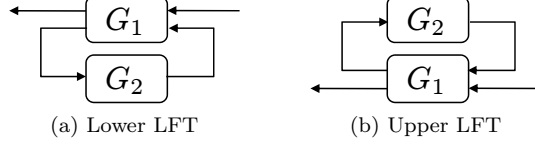
Figure 2: Linear fractional transformations (LFTs)

Figure 3: Picture of the Vector model PZT-actuated suspension used in our experimental setup

Positive definiteness (resp. semi-definiteness) of a symmetric matrix X will be denoted by $X \succ 0$ (resp. $X \succeq 0$), and a $\bullet$ in a symmetric matrix will represent a block which follows from symmetry.

For given (A, B, Q, R, S), where $Q = Q^T$ and $R = R^T$, we define the functions

$$\mathcal{R}_{(A,B,Q,R,S)}(P) \; := \; A^T P A + Q - (A^T P B + S)(B^T P B + R)^{-1}(B^T P A + S^T) \tag{2a}$$

$$\mathcal{K}_{(A,B,Q,R,S)}(P) \; := \; -(B^T P B + R)^{-1}(B^T P A + S^T). \tag{2b}$$

We will make the notation more compact in the remainder of the paper by respectively denoting these functions as $\mathcal{R}_\phi(P)$ and $\mathcal{K}_\phi(P)$ where ϕ is an appropriately defined 5-tuple. Note that the equation $\mathcal{R}_\phi(P) = P$ is a discrete algebraic Riccati equation (DARE). If $\mathcal{R}_\phi(P) = P = P^T$ and $A + B\mathcal{K}_\phi(P)$ is Schur, then P is called a stabilizing solution of the DARE. Throughout the paper, we will implicitly use the property that if a DARE has a stabilizing solution, it is unique [11].

A matrix pair (A, B) will be called d-stabilizable if $\exists K$ such that $A + BK$ is Schur. A matrix pair (A, C) will be called d-detectable if $\exists L$ such that $A + LC$ is Schur. For a given stable and causal LTI system G, its $\mathcal{H}_2$ and $\mathcal{H}_\infty$ norms will respectively be denoted as $\|G\|_2$ and $\|G\|_\infty$. For two causal LTI systems G_1 and G_2, we denote the lower linear fractional transformation (LFT) of G_1 by G_2 (shown in Fig. 2a) as $\mathcal{F}_l(G_1, G_2)$. We will denote the upper LFT of G_1 by G_2 (shown in Fig. 2b) as $\mathcal{F}_u(G_1, G_2)$.

2 Hard Disk Drive Model

In this section, we present the HDD model we will be using throughout this chapter. The HDD we are considering has the PZT-actuated suspension shown in Fig. 3, which is a Vector model suspension provided to us by Hutchinson Technology Inc. In our setup, we use a laser Doppler vibrometer (LDV) to measure the
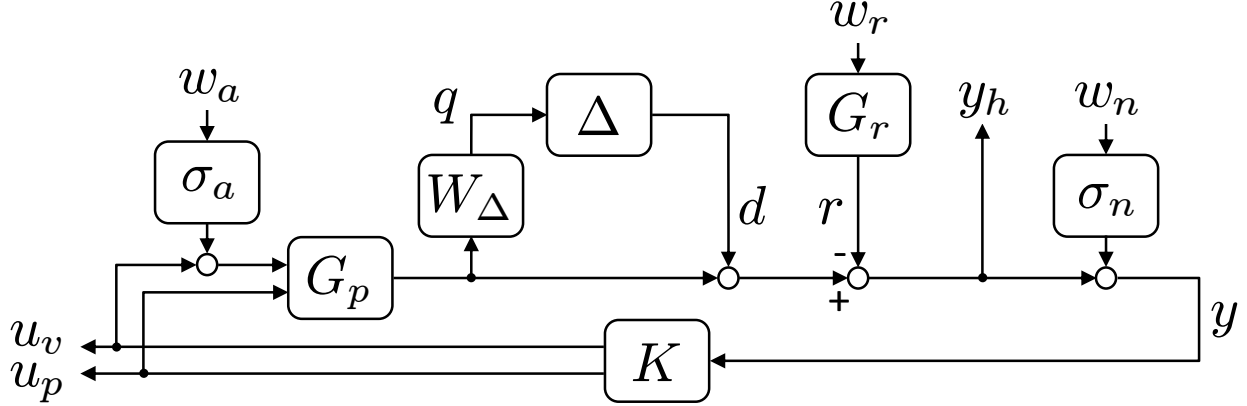
Figure 4: HDD block diagram

Table 1: HDD signals

Signal	Description	Units
r	Disturbances on the head position [8]	nm
u_p	PZT actuator control signal	V
u_v	Voice coil motor control signal	V
w_a	Airflow disturbances	(normalized)
w_n	PES sensor noise	(normalized)
w_r	Disturbances on the head position	(normalized)
y	PES	nm
y_h	Head displacement relative to the track center	nm

absolute radial displacement of the slider. The control circuits include a Texas Instrument TMS320C6713 DSP board and an in-house made analog board with a 12-bit ADC, a 12-bit DAC, a voltage amplifier to drive the MA, and a current amplifier to drive the voice coil motor. The DSP sampling period is 1.4×10^{-5} s and the controller delay, which includes ADC and DAC conversion delay and DSP computation delay, is 6μ s. A hole was cut through the case of the drive to allow the LDV laser to shine on the slider. It should be noted that these modifications affect the response of the drive and may have detrimentally affected the attainable performance of the servo system.

The block diagram of our HDD setup is shown in Fig. 4 and the relevant signals and their units are listed in Table 1. In this block diagram, we treat the dynamics from the two control inputs to the head displacement as a single block to take into account the knowledge that both actuators can excite the same vibration modes in the suspension. Exploiting this knowledge allows us to form a model which does not have redundant states resulting from including two copies of the suspension vibration modes. The block Δ is an unknown stable causal LTI system which satisfies $\|\Delta\|_\infty \leq 1$. This block, along with W_Δ, characterizes the output dynamic multiplicative uncertainty on G_p.

Table 2: Model parameters for G_p

mode, i	$\begin{bmatrix} a_{i,1} \\ a_{i,2} \end{bmatrix}$	B_i
1	$\begin{bmatrix} 1.99607 \\ -0.996286 \end{bmatrix}$	$\begin{bmatrix} 3.982 & 0 \\ -6.262 & 0 \end{bmatrix}$
2	$\begin{bmatrix} 1.474 \\ -0.9680 \end{bmatrix}$	$\begin{bmatrix} -1.415 & 1.263 \\ 1.368 & -1.659 \end{bmatrix}$
3	$\begin{bmatrix} 1.381 \\ -0.9762 \end{bmatrix}$	$\begin{bmatrix} -0.8049 & 2.338 \\ 2.082 & -0.01339 \end{bmatrix}$
4	$\begin{bmatrix} 0.5387 \\ -0.9632 \end{bmatrix}$	$\begin{bmatrix} 0.1366 & -4.740 \\ -1.520 & 25.62 \end{bmatrix}$
5	$\begin{bmatrix} 0.04209 \\ -0.9353 \end{bmatrix}$	$\begin{bmatrix} -0.06772 & 9.273 \\ -0.1826 & 105.8 \end{bmatrix}$
6	$\begin{bmatrix} -1.653 \\ -0.9527 \end{bmatrix}$	$\begin{bmatrix} -0.09272 & -1.618 \\ -0.1086 & -0.2218 \end{bmatrix}$

To construct a discrete-time model of our system, we used the methodology of [13]. To find the model of G_p, we first obtained frequency responses of our system from u_v to y and u_p to y. Using weighted least squares, we separately fit a continuous-time model to each of these frequency responses, which we then combined into a single model and used common mode identification [2] to eliminate redundant copies of the suspension vibration modes. We then discretized this model with the 6μ s delay on each of its two inputs to yield the model for G_p. This model is given by

$$G_p(z) = \begin{bmatrix} -0.6858 & 20.94 \end{bmatrix} z^{-1} + \sum_{i=1}^{6} \begin{bmatrix} 1 & 0 \end{bmatrix} \left(zI - \begin{bmatrix} a_{i,1} & 1 \\ a_{i,2} & 0 \end{bmatrix} \right)^{-1} B_i \tag{3}$$

where the model parameters are as listed in Table 2. Because there are two poles at $z = 0$—one for each input channel—the state-space model of G_p has 14 states. The poles at $z = 0$ were introduced by the discretization of the continuous-time input delay. The six vibration modes in (3) are ordered from lowest to highest resonance frequency. The Bode plot of this model is shown in Fig. 5.

The weighting for the dynamic multiplicative uncertainty of G_p, given by

$$W_\Delta = \frac{0.9733 - z}{z - 0.465}, \tag{4}$$

was chosen so that the uncertain model enveloped the experimental frequency response of G_p. The Bode magnitude plot of W_Δ is shown in Fig. 6a. Since Δ is a SISO system, upper and lower bounds on the

6

magnitude of each input/output pair in G_p can be easily computed one frequency at a time. Doing so yields the upper and lower bounds on the Bode magnitude plots of G_p shown in Fig. 7. The values $\sigma_a = 0.04854$ and $\sigma_n = 1.3$ were determined by matching the power spectrum density of the open loop slider motion respectively at low and high frequency. The disturbances on the head position are characterized by

$$
\begin{aligned}
G_r(z) &= \begin{bmatrix} 1 & 0 \end{bmatrix} \left(zI - \begin{bmatrix} 1.964 & 1 \\ -0.975 & 0 \end{bmatrix} \right)^{-1} \begin{bmatrix} -0.2574 \\ 0.25 \end{bmatrix} \\
&+ \begin{bmatrix} 1 & 1 \end{bmatrix} \left(zI - \begin{bmatrix} 0.9956 & -0.0745 \\ 0 & 0.9956 \end{bmatrix} \right)^{-1} \begin{bmatrix} -0.9533 \\ 0.919 \end{bmatrix}.
\end{aligned}
\tag{5}
$$

Figure 6b shows the Bode magnitude plot of G_r. In addition to capturing the effect of disturbances on the head position, this model of G_r also captures the low-frequency drift in the LDV position measurements resulting from integration of velocity measurements. The second-order mode near 1 kHz in this model captures the effect of disk modes between 1 kHz and 3 kHz.

These disturbances, although realistic for our experimental setup, are larger than the disturbances typically found in a HDD. First of all, the measurement noise of the LDV is somewhat larger than the measurement noise of the PES. Moreover, as we previously mentioned, the LDV has a significant low-frequency drift. These two factors along with the mechanical modifications of the drive significantly deteriorate the achievable level of closed-loop performance.

With some manipulation, the blocks in Fig. 4 can be grouped to form the LFT representation in Fig. 8. In this form G_H has 19 states. For the remainder of this chapter, we will use the balanced realization of G_H for analysis and control design.

3 H2 Guaranteed Cost Analysis

In this section, we review the results of [3] on $\mathcal{H}_2$ guaranteed cost analysis. In particular, we first present an SDP for determining the $\mathcal{H}_2$ guaranteed cost performance of a given system and then show that this convex optimization can be efficiently solved using nonlinear convex optimization involving Riccati equation solutions. For the sake of brevity and clarity of presentation, we do not present the proofs here; interested readers should read the paper cited above.
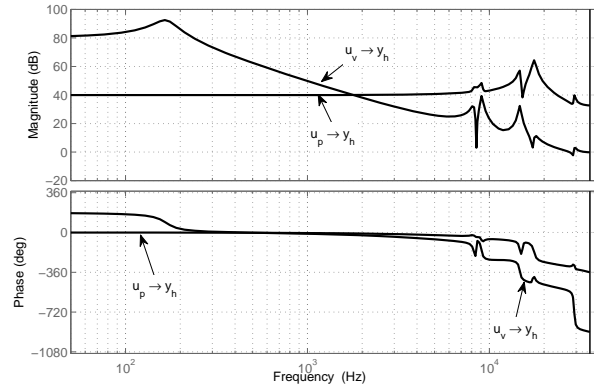
Figure 5: Bode plot of G_p

(a) W_Δ

(b) G_r
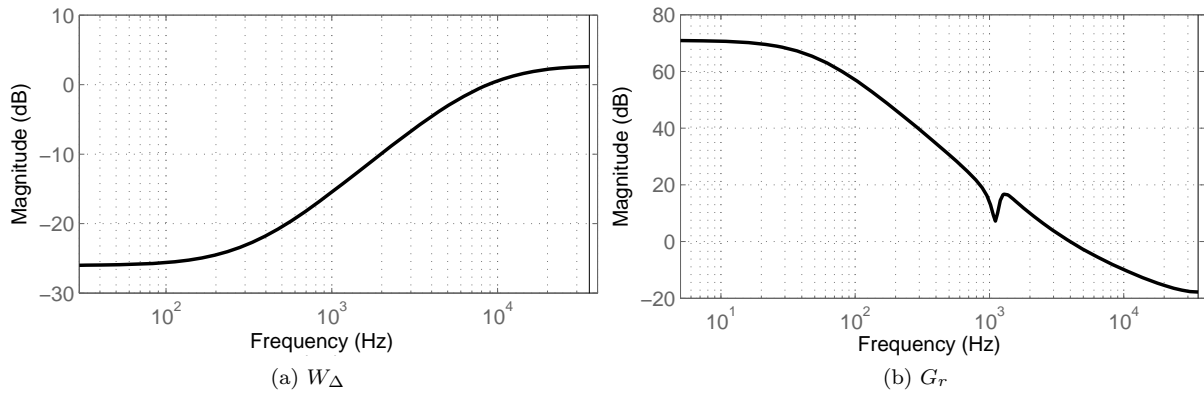
Figure 6: Bode magnitude plots of W_Δ and G_r

(a) $u_v \to y_h$

(b) $u_p \to y_h$
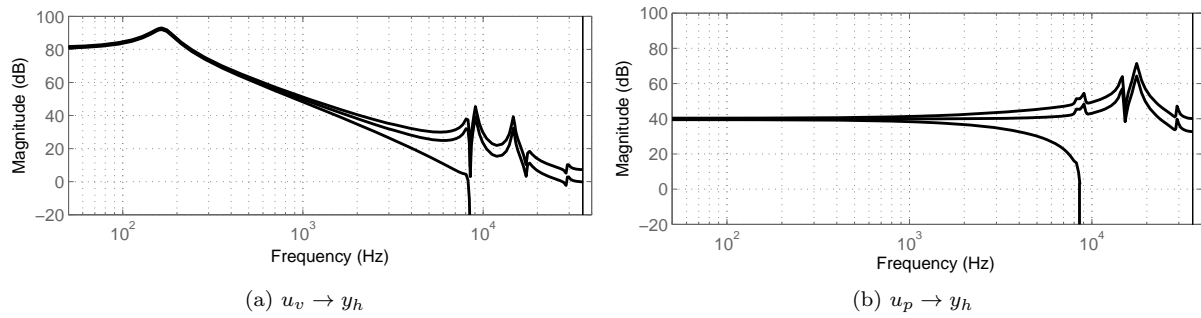
Figure 7: Nominal Bode magnitude plots for G_p along with pointwise upper and lower bounds over modeled uncertainty
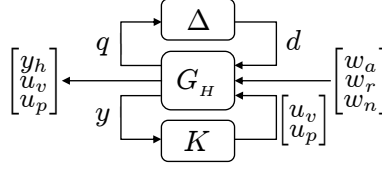
Figure 8: LFT representation of HDD model

3.1 Semi-Definite Programming Approach

Before considering systems with uncertainty, we first consider a given discrete-time LTI system $\tilde{G}$ with known state-space realization

$$\tilde{G} \sim \left[\begin{array}{c|c} A_{\tilde{G}} & B_{\tilde{G}} \\ \hline C_{\tilde{G}} & D_{\tilde{G}} \end{array} \right].$$ (6)

A well-known characterization of the $\mathcal{H}_2$ norm is that $\|\tilde{G}\|_2^2 < \gamma$ if and only if there exist $P \succ 0$ and W such that

$$\text{tr}\{W\} < \gamma$$ (7a)

$$W \succ B_{\tilde{G}}^T P B_{\tilde{G}} + D_{\tilde{G}}^T D_{\tilde{G}}$$ (7b)

$$P \succ A_{\tilde{G}}^T P A_{\tilde{G}} + C_{\tilde{G}}^T C_{\tilde{G}}.$$ (7c)

In this context, however, it is beneficial for us to consider an alternate characterization which says that $\|\tilde{G}\|_2^2 < \gamma$ if and only if there exist $P \succ 0, W, V$ such that

$$\text{tr}\{W\} < \gamma$$ (8a)

$$\left[\begin{array}{cc} P & V^T \\ V & W \end{array} \right] \succ \left[\begin{array}{cc} A_{\tilde{G}} & B_{\tilde{G}} \\ C_{\tilde{G}} & D_{\tilde{G}} \end{array} \right]^T \left[\begin{array}{cc} P & 0 \\ 0 & I \end{array} \right] \left[\begin{array}{cc} A_{\tilde{G}} & B_{\tilde{G}} \\ C_{\tilde{G}} & D_{\tilde{G}} \end{array} \right].$$ (8b)

It should be noted that eliminating V from (8b) using the matrix elimination technique (see, e.g., [1]) yields (7b)–(7c). This alternate characterization is more suitable for two reasons. First, as will be discussed later in this section, it will allow us to consider a richer set of system uncertainty models. Second, it will allow us to use the matrix variable elimination technique to derive an optimal control scheme in Sect. 4, which will be important in our approaches to the output feedback problem developed in Sect. 5.

We now turn our attention to analyzing the $\mathcal{H}_2$ performance of the system interconnection shown in Fig. 9 where $\bar{G}$ has the state-space realization
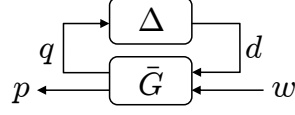
Figure 9: LFT representation of uncertain system

$$\bar{G} \sim \left[\begin{array}{c|cc} \bar{A} & \bar{B}_1 & \bar{B}_2 \\ \hline \bar{C}_1 & \bar{D}_{11} & \bar{D}_{12} \\ \bar{C}_2 & \bar{D}_{21} & \bar{D}_{22} \end{array}\right] \tag{9}$$

and Δ is a real matrix satisfying $\|\Delta\| \leq 1$. Closing the loop yields

$$
\begin{aligned}
\mathcal{F}_u(\bar{G}, \Delta) \quad &\sim \quad \left[\begin{array}{c|c} \bar{A} + \bar{B}_1(I - \Delta\bar{D}_{11})^{-1}\Delta\bar{C}_1 & \bar{B}_2 + \bar{B}_1(I - \Delta\bar{D}_{11})^{-1}\Delta\bar{D}_{12} \\ \hline \bar{C}_2 + \bar{D}_{21}(I - \Delta\bar{D}_{11})^{-1}\Delta\bar{C}_1 & \bar{D}_{22} + \bar{D}_{21}(I - \Delta\bar{D}_{11})^{-1}\Delta\bar{D}_{12} \end{array}\right] \\
&=: \quad \left[\begin{array}{c|c} A_\Delta & B_\Delta \\ \hline C_\Delta & D_\Delta \end{array}\right].
\end{aligned} \tag{10}
$$

We are thus interested in determining if $\|\mathcal{F}_u(\bar{G}, \Delta)\|_2^2 < \gamma$, $\forall\|\Delta\| \leq 1$. Using the characterization of the $\mathcal{H}_2$ norm given by (8), we would like to know if there exists $P \succ 0, W, V$ such that $\mathrm{tr}\{W\} < \gamma$ and

$$\left[\begin{array}{cc} P & V^T \\ V & W \end{array}\right] \succ \left[\begin{array}{cc} A_\Delta & B_\Delta \\ C_\Delta & D_\Delta \end{array}\right]^T \left[\begin{array}{cc} P & 0 \\ 0 & I \end{array}\right] \left[\begin{array}{cc} A_\Delta & B_\Delta \\ C_\Delta & D_\Delta \end{array}\right], \qquad \forall\|\Delta\| \leq 1 . \tag{11}$$

It should be noted that, although the state-space matrices are a function of Δ, the analysis variables (P, W, and V) are not. Applying the S-procedure (see, e.g., [1]) to (11) yields the equivalent condition that there exists $\tau > 0, P \succ 0, W, V$ such that $\mathrm{tr}\{W\} < \gamma$ and

$$\mathcal{M}(\tau, P, W, V) := \left[\begin{array}{ccc} P & 0 & V^T \\ 0 & \tau I & 0 \\ V & 0 & W \end{array}\right] - \left[\begin{array}{ccc} \bar{A} & \bar{B}_1 & \bar{B}_2 \\ \bar{C}_1 & \bar{D}_{11} & \bar{D}_{12} \\ \bar{C}_2 & \bar{D}_{21} & \bar{D}_{22} \end{array}\right]^T \left[\begin{array}{ccc} P & 0 & 0 \\ 0 & \tau I & 0 \\ 0 & 0 & I \end{array}\right] \left[\begin{array}{ccc} \bar{A} & \bar{B}_1 & \bar{B}_2 \\ \bar{C}_1 & \bar{D}_{11} & \bar{D}_{12} \\ \bar{C}_2 & \bar{D}_{21} & \bar{D}_{22} \end{array}\right] \succ 0 . \tag{12}$$

By Schur complements, this is equivalent to the existence of τ, P, W, V such that

$$\bar{\mathcal{M}}(\tau, P, W, V) := \begin{bmatrix} P & \bullet & \bullet & \bullet & \bullet & \bullet \\ 0 & \tau I & \bullet & \bullet & \bullet & \bullet \\ V & 0 & W & \bullet & \bullet & \bullet \\ P\bar{A} & P\bar{B}_1 & P\bar{B}_2 & P & \bullet & \bullet \\ \tau\bar{C}_1 & \tau\bar{D}_{11} & \tau\bar{D}_{12} & 0 & \tau I & \bullet \\ \bar{C}_2 & \bar{D}_{21} & \bar{D}_{22} & 0 & 0 & I \end{bmatrix} \succ 0 . \tag{13}$$

These two new conditions, which are equivalent to each other, remove the dependence of the matrices on Δ at the expense of introducing an extra scalar parameter, τ. Since the matrices in the two new conditions do not depend on Δ, they give us computationally tractable means to verify that γ is an upper bound on the worst-case $\mathcal{H}_2$ performance of $\mathcal{F}_u(\bar{G}, \Delta)$ when Δ is a real matrix satisfying $\|\Delta\| \leq 1$.

Rewriting these feasibility problems as an optimization problems to find the smallest upper bound of this type yields

$$\inf_{\tau > 0, P \succ 0, W, V} \operatorname{tr}\{W\} \quad \text{s.t.} \quad \mathcal{M}(\tau, P, W, V) \succ 0 \tag{14}$$

$$\inf_{\tau, P, W, V} \operatorname{tr}\{W\} \quad \text{s.t.} \quad \bar{\mathcal{M}}(\tau, P, W, V) \succ 0 . \tag{15}$$

We will refer to the square root of the value of these optimization problems as the $\mathcal{H}_2$ guaranteed cost of $\bar{G}$. Of these two optimizations, (14) is more useful for determining the $\mathcal{H}_2$ guaranteed cost of a given system because its matrix inequalities are smaller in dimension and the optimization problem has fewer dual variables. However, as we will see in Sects. 4 and 5, (15) will be more suitable for control design. Relaxing the strict inequalities in either of these optimization problems to non-strict inequalities results in a SDP. Thus, a reasonable way to solve the $\mathcal{H}_2$ guaranteed cost analysis problem is to relax (14) to a SDP then solve the SDP using an appropriate solver.

From the derivation, it is obvious that the $\mathcal{H}_2$ guaranteed cost is an upper bound on the worst-case $\mathcal{H}_2$ performance of the interconnection in Fig. 9 when Δ is a real matrix satisfying $\|\Delta\| \leq 1$. What is not immediately apparent, however, is that the $\mathcal{H}_2$ guaranteed cost is also an upper bound on the worst-case $\mathcal{H}_2$ performance of the interconnection in Fig. 9 when Δ is only known to be a causal LTI system satisfying $\|\Delta\|_\infty \leq 1$.

3.2 Riccati Equation Approach

We begin this subsection by noting that (14) can equivalently be expressed as

$$\inf_{\tau > 0} J_\tau(\bar{G}) \tag{16}$$

where

$$J_\tau(\bar{G}) := \inf_{P \succ 0, W, V} \text{tr}\{W\} \quad \text{s.t.} \quad \mathcal{M}(\tau, P, W, V) \succ 0 . \tag{17}$$

It can be shown that $J_\tau(\bar{G})$ is well-defined, i.e. for a fixed value of $\tau > 0$, $J_\tau(\bar{G})$ is independent of the realization of $\bar{G}$.

Whenever the optimization problem (17) is infeasible for a particular value of τ, we will say that $J_\tau(\bar{G}) = \infty$. Defining

$$\begin{bmatrix} \bar{Q} & \bar{S} \end{bmatrix} := \bar{C}_2^T \begin{bmatrix} \bar{C}_2 & \bar{D}_{21} \end{bmatrix} + \tau \bar{C}_1^T \begin{bmatrix} \bar{C}_1 & \bar{D}_{11} \end{bmatrix} \tag{18a}$$

$$\begin{bmatrix} \bar{Q}_W & \bar{S}_W \end{bmatrix} := \bar{D}_{22}^T \begin{bmatrix} \bar{D}_{22} & \bar{D}_{21} \end{bmatrix} + \tau \bar{D}_{12}^T \begin{bmatrix} \bar{D}_{12} & \bar{D}_{11} \end{bmatrix} \tag{18b}$$

$$\bar{R} := \bar{D}_{21}^T \bar{D}_{21} + \tau(\bar{D}_{11}^T \bar{D}_{11} - I) \tag{18c}$$

$$\bar{\phi} := (\bar{A}, \bar{B}_1, \bar{Q}, \bar{R}, \bar{S}) \tag{18d}$$

$$\bar{\psi} := (\bar{B}_2, \bar{B}_1, \bar{Q}_W, \bar{R}, \bar{S}_W) \tag{18e}$$

it was shown [3] that $J_\tau(\bar{G}) \neq \infty$ if and only if the DARE $\mathcal{R}_{\bar{\phi}}(P) = P$ has a stabilizing solution, P_0, such that $\bar{B}_1^T P_0 \bar{B}_1 + \bar{R} \prec 0$. In this case,

$$J_\tau(\bar{G}) = \text{tr}\{\mathcal{R}_{\bar{\psi}}(P_0)\} . \tag{19}$$

It was also shown that if $J_\tau(\bar{G}) \neq \infty$ for $\tau = \tau_0$, then $J_\tau \neq \infty$ for all $\tau > \tau_0$. Moreover, there exists a value of τ such that $J_\tau(\bar{G}) \neq \infty$ if and only if the interconnection in Fig. 9 is robustly stable over $\|\Delta\|_\infty \leq 1$, i.e. the $\mathcal{H}_\infty$ norm of $\bar{G}$ from d to q is less than 1. This condition is in turn equivalent to the DARE $\mathcal{R}_\rho(P) = P$ having a stabilizing solution P_0 such that $\bar{B}_1^T P_0 \bar{B}_1 + \bar{D}_{11}^T \bar{D}_{11} - I \prec 0$ where

$$\rho := (\bar{A}, \ \bar{B}_1, \ \bar{C}_1^T \bar{C}_1, \ \bar{D}_{11}^T \bar{D}_{11} - I, \ \bar{C}_1^T \bar{D}_{11}) . \tag{20}$$

Thus, once we have verified that the optimization problem (16) is feasible by using the DARE $\mathcal{R}_\rho(P) = P$, we can always find values of τ for which $J_\tau(\bar{G}) \neq \infty$ simply by making τ increasingly large.

With this in mind, we would like to know how $J_\tau(\bar{G})$ varies as τ varies. First, since minimizing a convex

function of several variables over a subset of those variables produces a convex function of the remaining variables, we see that $J_\tau(\bar{G})$ is a convex nonlinear function of τ. Second, since the stabilizing solution of a DARE is analytic in its parameters [5] and $J_\tau(\bar{G})$ is an analytic function of the stabilizing DARE solution, $J_\tau(\bar{G})$ is an analytic function of τ. We will therefore find the global optimal value of $J_\tau(\bar{G})$ by finding a value of τ such that $(d/d\tau)(J_\tau(\bar{G})) = 0$.

Although the most straightforward way to find $(d/d\tau)(J_\tau(\bar{G}))$ is by directly taking the derivative of the relevant equations with respect to τ, as was done in [3], we will pursue a slightly different approach here which is more computationally efficient. First, we define $\epsilon := \tau^{-1}$ and

$$\hat{\phi} \;\; := \;\; (\bar{A},\; \bar{B}_1,\; \epsilon\bar{Q},\; \epsilon\bar{R},\; \epsilon\bar{S}) \tag{21a}$$

$$\hat{\psi} \;\; := \;\; (\bar{B}_2,\; \bar{B}_1,\; \epsilon\bar{Q}_W,\; \epsilon\bar{R},\; \epsilon\bar{S}_W)\,. \tag{21b}$$

Multiplying the DARE by ϵ yields $\mathcal{R}_{\hat{\phi}}(\epsilon P_0) = \epsilon P_0$. Also note that $\epsilon\mathcal{R}_{\bar{\psi}}(P_0) = \mathcal{R}_{\hat{\psi}}(\epsilon P_0)$. Taking derivatives of these two equations yields, after some algebra, that

$$
\begin{aligned}
\frac{d}{d\epsilon}(\epsilon P_0) \;\; &= \;\; \left(\bar{A} + \bar{B}_1\mathcal{K}_{\bar{\phi}}(P_0)\right)^T \frac{d}{d\epsilon}(\epsilon P_0)\left(\bar{A} + \bar{B}_1\mathcal{K}_{\bar{\phi}}(P_0)\right) \\
&\quad + \left(\bar{C}_2 + \bar{D}_{21}\mathcal{K}_{\bar{\phi}}(P_0)\right)^T\left(\bar{C}_2 + \bar{D}_{21}\mathcal{K}_{\bar{\phi}}(P_0)\right)
\end{aligned} \tag{22a}
$$

$$
\begin{aligned}
\frac{d}{d\epsilon}\left(\epsilon\mathcal{R}_{\bar{\psi}}(P_0)\right) \;\; &= \;\; \left(\bar{B}_2 + \bar{B}_1\mathcal{K}_{\bar{\psi}}(P_0)\right)^T \frac{d}{d\epsilon}(\epsilon P_0)\left(\bar{B}_2 + \bar{B}_1\mathcal{K}_{\bar{\psi}}(P_0)\right) \\
&\quad + \left(\bar{D}_{22} + \bar{D}_{21}\mathcal{K}_{\bar{\psi}}(P_0)\right)^T\left(\bar{D}_{22} + \bar{D}_{21}\mathcal{K}_{\bar{\psi}}(P_0)\right)\,.
\end{aligned} \tag{22b}
$$

The first of these equations is a discrete Lyapunov equation for $(d/d\epsilon)(\epsilon P_0)$. Since $\bar{A} + \bar{B}_1\mathcal{K}_{\bar{\phi}}(P_0)$ is stable (by the definition of a stabilizing solution of a DARE), we see that there exists upper triangular $\bar{U}$ such that $\bar{U}^T\bar{U} = (d/d\epsilon)(\epsilon P_0)$ and we can directly solve for $\bar{U}$ using the `dlyapchol` function in MATLAB. Using this, we express

$$\mathrm{tr}\left\{\frac{d}{d\epsilon}(\epsilon\mathcal{R}_{\bar{\psi}}(P_0))\right\} = \|\bar{U}(\bar{B}_2 + \bar{B}_1\mathcal{K}_{\bar{\psi}}(P_0))\|_F^2 + \|\bar{D}_{22} + \bar{D}_{21}\mathcal{K}_{\bar{\psi}}(P_0)\|_F^2\,. \tag{23}$$

Using the chain rule, we see that

$$\frac{d}{d\epsilon}(\epsilon\mathcal{R}_{\bar{\psi}}(P_0)) = \mathcal{R}_{\bar{\psi}}(P_0) + \epsilon\frac{d}{d\epsilon}(\mathcal{R}_{\bar{\psi}}(P_0))\,. \tag{24}$$

Thus, taking the derivative of (19) and applying the chain rule to the right-hand side yields

$$\frac{d}{d\tau}(J_\tau(\bar{G})) = -\tau^{-2}\mathrm{tr}\left\{\frac{d}{d\epsilon}(\mathcal{R}_{\bar{\psi}}(P_0))\right\} = \tau^{-1}\mathrm{tr}\left\{\mathcal{R}_{\bar{\psi}}(P_0) - \frac{d}{d\epsilon}(\epsilon\mathcal{R}_{\bar{\psi}}(P_0))\right\}\,. \tag{25}$$
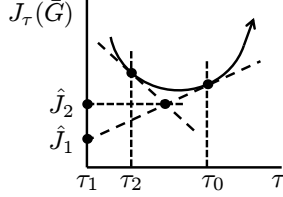
Figure 10: Illustration of lower bound computation in $\mathcal{H}_2$ guaranteed cost analysis

Therefore, we have that

$$\frac{d}{d\tau}(J_\tau(\bar{G})) = \frac{1}{\tau}\left(J_\tau(\bar{G}) - \|\bar{U}(\bar{B}_2 + \bar{B}_1\mathcal{K}_{\bar{\psi}}(P_0))\|_F^2 - \|\bar{D}_{22} + \bar{D}_{21}\mathcal{K}_{\bar{\psi}}(P_0)\|_F^2\right). \tag{26}$$

In comparison to formulas given in [3], using (26) to compute the cost derivative is more computationally efficient because it requires fewer matrix multiplications and additions.

The value and derivative of $J_\tau(\bar{G})$ is also useful for generating a lower bound on the optimal value of (16). Consider Fig. 10, which shows a representative graph of $J_\tau(\bar{G})$ in which τ_0 is known to be an upper bound on the minimizing value of τ. By convexity, if τ_1 is known to be a lower bound on the minimizing value of τ, the value and derivative of $J_\tau(\bar{G})$ at τ_0 gives us the lower bound $\hat{J}_1$. If instead, the value and derivative of $J_\tau(\bar{G})$ at τ_0 and τ_2 is known, we have the lower bound $\hat{J}_2$. These lower bounds are respectively given by

$$\begin{aligned}
\hat{J}_1 &= J_{\tau_0} - m_0(\tau_0 - \tau_1) & \text{(27a)} \\
\hat{J}_2 &= \frac{m_2[m_0(\tau_0 - \tau_2) - (J_{\tau_0} - J_{\tau_2})]}{m_0 - m_2} + J_{\tau_2} & \text{(27b)}
\end{aligned}$$

where J_{τ_i} is interpreted as $J_\tau(\bar{G})$ evaluated at $\tau = \tau_i$ and m_i is $(d/d\tau)(J_\tau(\bar{G}))$ evaluated at $\tau = \tau_i$. It should be noted that the second of these lower bounds is less conservative when it is applicable.

With these results in place, we can easily solve (16) using the following methodology:

1. **Check Feasibility:** Check that the DARE $\mathcal{R}_\rho(P) = P$ has a stabilizing solution P_0 such that $\bar{B}_1^T P_0 \bar{B}_1 + \bar{D}_{11}^T \bar{D}_{11} - I \prec 0$.

2. **Find Initial Interval:** Choose $\alpha > 1$. As previously noted, the DARE $\mathcal{R}_{\bar{\phi}}(P) = P$ will have a stabilizing solution with the required properties for $\tau = \alpha^k$, for large enough k. Starting from $k = 0$, iterate over increasing k until a value of $\tau = \alpha^k$ is found such that the DARE has a stabilizing solution P_0 that satisfies $\bar{B}_1^T P_0 \bar{B}_1 + \bar{R} \prec 0$ and $(d/d\tau)(J_\tau(\bar{G})) > 0$. Denote this value of τ by τ_u. Note that this corresponds to an upper bound on the optimal value of τ. If $\tau_u = 1$, then 0 is a lower bound on the optimal value of τ, otherwise τ_u/α is a lower bound.

14

3. **Bisection:** Solve the equation $(d/d\tau)(J_\tau(\bar{G})) = 0$ over τ using bisection. Use (26) for evaluating $(d/d\tau)(J_\tau(\bar{G}))$. Whenever the DARE $\mathcal{R}_{\bar{\phi}}(P) = P$ does not have a stabilizing solution with the required properties for a given value of τ, this corresponds to a lower bound on the optimal value of τ.

In our implementation, we use $\alpha = 100$. Also, except when the lower bound on the optimal value of τ is 0, we use the geometric mean instead of the arithmetic mean to better deal with large intervals in which the optimal value of τ could lie. We use two stopping criteria in our implementation. If we define the relative error as $\nu := 1 - \underline{J}/J_\tau(\bar{G})$ where $\underline{J}$ is the lower bound computed by (27), we terminate the algorithm when either $\nu < 10^{-10}$ or 30 iterations have been executed in steps 2–3.

3.3   Application to Hard Disk Drives

So far in this section, we have developed two methodologies for analyzing the robust performance of a system with dynamic uncertainty—one based on the solution of a SDP and another based on nonlinear convex optimization involving Riccati equation solutions. We will now use these two methodologies to examine the performance of a closed-loop HDD system for a specified controller.

For the controller, we choose the controller returned by the MATLAB Robust Control Toolbox function `hinfsyn` applied to the optimization problem

$$\inf_K \left\| \mathcal{F}_l(\hat{G}_H, K) \right\|_\infty \tag{28}$$

where $\hat{G}_H := \mathrm{diag}[0.001, 0.001, 1, 1, 1]G_H$. The controller returned by `hinfsyn`, K^o, contained 19 states and achieved $\|\mathcal{F}_l(\hat{G}_H, K^o)\|_\infty = 0.3831$. For this controller, the nominal $\mathcal{H}_2$ norm of the interconnection in Fig. 8 (i.e. with $\Delta = 0$) was 11.6212.

We used three approaches to find the $\mathcal{H}_2$ guaranteed cost of the system $G_{cl} := \mathcal{F}_l(G_H, K^o)$: solving the SDP (14) using the `mincx` command, solving (14) using SeDuMi and YALMIP, and solving (16) using the methodology at the end of Sect. 3.2. We will refer to the latter of these approaches as the DARE approach. Using these three approaches to analyze the performance of this 38th-order system yielded the results listed in Table 3. Although all three approaches yielded similar values of the $\mathcal{H}_2$ guaranteed cost and the corresponding value of τ, the DARE approach was more than 100 times faster for this system than the other two approaches.

We now look more closely at the results of applying the DARE approach to this problem. In particular, we are interested in the values of $J_\tau(G_{cl})$ and $(d/d\tau)(J_\tau(G_{cl}))$ as functions of τ. Figure 11 shows a plot of these two quantities for 50 linearly spaced points in the interval $[2, 6]$ along with an estimate of $(d/d\tau)(J_\tau(G_{cl}))$

15

Table 3: Analysis of closed-loop HDD performance using three approaches

Approach	Optimization Time (s)	$\mathcal{H}_2$ Guaranteed Cost	Optimal τ
mincx	147.0465	17.3455	3.3997
SeDuMi	88.1718	17.345	3.3994
DARE	0.8112	17.3451	3.3995
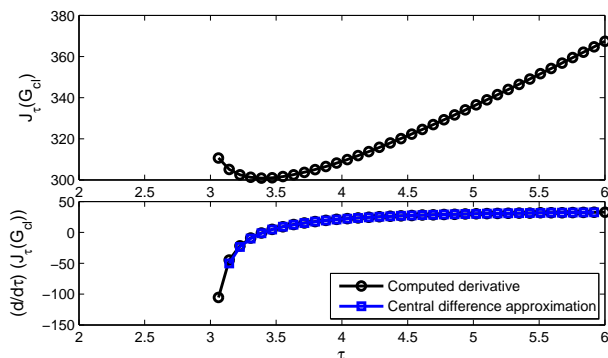
Figure 11: $J_\tau(G_{cl})$, the computed value of $(d/d\tau)(J_\tau(G_{cl}))$, and the central difference approximation to $(d/d\tau)(J_\tau(G_{cl}))$

obtained by applying the central difference approximation to $J_\tau(G_{cl})$. As we would expect, the curves are smooth, $(d/d\tau)(J_\tau(G_{cl}))$ is monotonic non-decreasing, and the computed values of $(d/d\tau)(J_\tau(G_{cl}))$ agree with the central difference approximations. It is interesting to note that as τ becomes large, $(d/d\tau)(J_\tau(G_{cl}))$ becomes constant and J_τ varies linearly with τ.

The $\mathcal{H}_2$ guaranteed costs computed so far reflect a combination of the "sizes" of the signals y_h, u_v, and u_p. However, it is more meaningful to look at the "sizes" of these three signals separately. To do so, we removed the outputs we are not interested in and computed the $\mathcal{H}_2$ guaranteed cost. For example, when we were interested in the $\mathcal{H}_2$ guaranteed cost associated with y_h, we removed the outputs u_v and u_p from G_{cl} and then computed the $\mathcal{H}_2$ guaranteed cost of the resulting system using the DARE approach. Doing this for y_h, u_v, and u_p yielded the $\mathcal{H}_2$ guaranteed costs given in Table 4. So, for the controller K^o, there very little control effort is used to achieve this level of robust position error performance.

Table 4: Closed-loop HDD performance

Signal	$\mathcal{H}_2$ Guaranteed Cost
y_h	17.3450nm
u_v	0.0440V
u_m	0.0052V
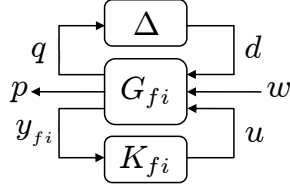
Figure 12: LFT representation of $\mathcal{H}_2$ guaranteed cost control structure

4 Full Information H2 Guaranteed Cost Control

In this section, we show how to use the analysis results of the previous section to design controllers which optimize the $\mathcal{H}_2$ guaranteed cost. The particular control design problem we consider is the full information control problem in which the controller has access to the state of the system and the disturbances acting on the system. We first present an SDP for determining an optimal controller and then show that, as in the previous section, this convex optimization can be efficiently solved using nonlinear convex optimization involving DARE solutions. The results in this section are taken from [4]. Again, for the sake of brevity and clarity of presentation, we do not present the proofs here; interested readers should read the paper cited above.

4.1 Semi-Definite Programming Approach

We begin by letting G_{fi} in Fig. 12, have the known state-space realization

$$
G_{fi} \sim \left[\begin{array}{c|ccc}
A & B_1 & B_2 & B_3 \\
\hline
C_1 & D_{11} & D_{12} & D_{13} \\
C_2 & D_{21} & D_{22} & D_{23} \\
\begin{bmatrix} I \\ 0 \\ 0 \end{bmatrix} & \begin{bmatrix} 0 \\ I \\ 0 \end{bmatrix} & \begin{bmatrix} 0 \\ 0 \\ I \end{bmatrix} & \begin{bmatrix} 0 \\ 0 \\ 0 \end{bmatrix}
\end{array} \right] .
\tag{29}
$$

This corresponds to letting

$$
y_{fi} = \begin{bmatrix} x_{fi} \\ d \\ w \end{bmatrix}
\tag{30}
$$

in Fig. 12 where x_{fi} is the state variable of G_{fi}. In this context, we are interested in finding a controller K_{fi} that achieves the best possible $\mathcal{H}_2$ guaranteed cost using this information. We will refer to this as the full information control problem.

17

It has been shown for the full information control problem that, given any state-space controller, it is always possible to construct a static gain controller which achieves the same $\mathcal{H}_2$ guaranteed cost. This allows us, without any loss of closed-loop performance, to consider only controllers of the form

$$u = K_x x + K_d d + K_w w \tag{31}$$

where K_x, K_d, and K_w are static gains. Equivalently, we make the restriction $K_{fi} = [K_x \ K_d \ K_w]$. Thus, we are interested in closed-loop systems of the form

$$\mathcal{F}_l(G_{fi}, K_{fi}) \sim \left[\begin{array}{c|cc} A + B_3 K_x & B_1 + B_3 K_d & B_2 + B_3 K_w \\ \hline C_1 + D_{13} K_x & D_{11} + D_{13} K_d & D_{12} + D_{13} K_w \\ C_2 + D_{23} K_x & D_{21} + D_{23} K_d & D_{22} + D_{23} K_w \end{array} \right] . \tag{32}$$

In particular, we would like to find K_x, K_d, and K_w such that $\mathcal{F}_l(G_{fi}, K_{fi})$ achieves the best possible $\mathcal{H}_2$ guaranteed cost.

Using the change of variables

$$\hat{P} \quad := \quad P^{-1} \tag{33a}$$

$$\hat{V} \quad := \quad V P^{-1} \tag{33b}$$

$$\epsilon \quad := \quad \tau^{-1} \tag{33c}$$

$$\hat{K}_x \quad := \quad K_x P^{-1} \tag{33d}$$

$$\hat{K}_d \quad := \quad \tau^{-1} K_d \tag{33e}$$

with the $\mathcal{H}_2$ guaranteed cost characterization (15) applied to $\mathcal{F}_l(G_{fi}, K_{fi})$ yields, after multiplying $\bar{\mathcal{M}}$ on the left and right by $\mathrm{diag}[P^{-1}, \tau^{-1}I, I, P^{-1}, \tau^{-1}I, I]$, the optimization problem

$$\inf_{\epsilon, \hat{P}, W, \hat{V}, \hat{K}_x, \hat{K}_d, K_w} \mathrm{tr}\{W\} \quad \text{s.t.} \quad \mathcal{M}_{fi}(\epsilon, \hat{P}, W, \hat{V}, \hat{K}_x, \hat{K}_d, K_w) \succ 0 \tag{34}$$

where

$$\mathcal{M}_{fi} := \begin{bmatrix} \hat{P} & \bullet & & \bullet & & \bullet & \bullet & \bullet \\ 0 & \epsilon I & & \bullet & & \bullet & \bullet & \bullet \\ \hat{V} & 0 & & W & & \bullet & \bullet & \bullet \\ A\hat{P} + B_3\hat{K}_x & \epsilon B_1 + B_3\hat{K}_d & & B_2 + B_3 K_w & & \hat{P} & \bullet & \bullet \\ C_1\hat{P} + D_{13}\hat{K}_x & \epsilon D_{11} + D_{13}\hat{K}_d & & D_{12} + D_{13}K_w & & 0 & \epsilon I & \bullet \\ C_2\hat{P} + D_{23}\hat{K}_x & \epsilon D_{21} + D_{23}\hat{K}_d & & D_{22} + D_{23}K_w & & 0 & 0 & I \end{bmatrix}. \tag{35}$$

For any feasible $\epsilon, \hat{P}, W, \hat{V}, \hat{K}_x, \hat{K}_d, K_w$, a controller which achieves the squared $\mathcal{H}_2$ guaranteed cost $\mathrm{tr}\{W\}$ (or better) is given by

$$K_{fi} = \begin{bmatrix} \hat{K}_x\hat{P}^{-1} & \epsilon^{-1}\hat{K}_d & K_w \end{bmatrix}. \tag{36}$$

If the strict inequality in (34) is relaxed to a non-strict inequality, the optimization becomes a SDP. Thus, a reasonable way to solve the optimal full information control problem is to relax (34) to a SDP, solve the SDP using an appropriate solver, and then reconstruct the controller using (36).

4.2 Riccati Equation Approach

In this subsection, we examine the optimal full information control problem when the following so-called regularity conditions hold:

- $D_{13}^T D_{13} + D_{23}^T D_{23}$ is invertible

- (A, B_3) is d-stabilizable

- (A_{fi}, C_{fi}) is d-detectable for all $\epsilon > 0$ where

$$A_{fi} := A - B_3(D_{13}^T D_{13} + \epsilon D_{23}^T D_{23})^{-1}(D_{13}^T C_1 + \epsilon D_{23}^T C_2) \tag{37a}$$

$$C_{fi} := \begin{bmatrix} C_1 \\ C_2 \end{bmatrix} - \begin{bmatrix} D_{13} \\ D_{23} \end{bmatrix} (D_{13}^T D_{13} + \epsilon D_{23}^T D_{23})^{-1}(D_{13}^T C_1 + \epsilon D_{23}^T C_2). \tag{37b}$$

As in the previous section, we begin by writing the relevant convex optimization problem as a nested optimization problem. In particular, we express (34) as

$$\inf_{\epsilon > 0} J_{fi,\epsilon} \tag{38}$$

19

where

$$J_{fi,\epsilon} := \inf_{\hat{P} \succ 0, W, \hat{V}, \hat{K}_x, \hat{K}_d, K_w} \text{tr}\{W\} \quad \text{s.t.} \quad \mathcal{M}_{fi}(\epsilon, \hat{P}, W, \hat{V}, \hat{K}_x, \hat{K}_d, K_w) \succ 0 . \tag{39}$$

Whenever (39) is infeasible for a particular value of ϵ, we will say that $J_{fi,\epsilon} = \infty$. Note that, since $\epsilon = \tau^{-1}$, performing the optimization (39) is the same as optimizing $J_\tau(\mathcal{F}_l(G_{fi}, K_{fi}))$ via choice of K_{fi} for $\tau = \epsilon^{-1}$.

Defining

$$\left[\, Q \mid S \,\right] := C_1^T \left[\, C_1 \mid D_{11} \quad D_{13} \,\right] + \epsilon C_2^T \left[\, C_2 \mid D_{21} \quad D_{23} \,\right] \tag{40a}$$

$$\left[\, Q_W \mid S_W \,\right] := D_{12}^T \left[\, D_{12} \mid D_{11} \quad D_{13} \,\right] + \epsilon D_{22}^T \left[\, D_{22} \mid D_{21} \quad D_{23} \,\right] \tag{40b}$$

$$R := \begin{bmatrix} R_{11} & \bullet \\ R_{21} & R_{22} \end{bmatrix} := \begin{bmatrix} D_{11}^T D_{11} - I & \bullet \\ D_{13}^T D_{11} & D_{13}^T D_{13} \end{bmatrix} + \epsilon \begin{bmatrix} D_{21}^T D_{21} & \bullet \\ D_{23}^T D_{21} & D_{23}^T D_{23} \end{bmatrix} \tag{40c}$$

$$\phi := (A, [B_1 \ B_3], Q, R, S) \tag{40d}$$

$$\psi := (B_2, [B_1 \ B_3], Q_W, R, S_W) \tag{40e}$$

it was shown [4] that $J_{fi,\epsilon} \neq \infty$ if and only if the DARE $\mathcal{R}_\phi(P) = P$ has a stabilizing solution $P_0 \succeq 0$ such that the factorization

$$\begin{bmatrix} B_1^T \\ B_3^T \end{bmatrix} P_0 \begin{bmatrix} B_1 & B_3 \end{bmatrix} + \begin{bmatrix} R_{11} & \bullet \\ R_{21} & R_{22} \end{bmatrix} = \begin{bmatrix} T_{21}^T T_{21} - T_{11}^T T_{11} & \bullet \\ T_{22}^T T_{21} & T_{22}^T T_{22} \end{bmatrix} \tag{41}$$

exists with T_{11} and T_{22} invertible. In this case, $J_{fi,\epsilon} = \epsilon^{-1}\text{tr}\{\mathcal{R}_\psi(P_0)\}$ and the optimal values of the controller parameters are

$$\begin{bmatrix} K_x^o & K_d^o & K_w^o \end{bmatrix} := -(B_3^T P_0 B_3 + R_{22})^{-1} \begin{bmatrix} B_3^T P_0 & D_{13}^T & \epsilon D_{23}^T \end{bmatrix} \begin{bmatrix} A & B_1 & B_2 \\ C_1 & D_{11} & D_{12} \\ C_2 & D_{21} & D_{22} \end{bmatrix} . \tag{42}$$

If the factorization (41) exists, then it can be formed using the following steps:

1. Perform the Cholesky factorization $T_{22}^T T_{22} = B_3^T P_0 B_3 + R_{22}$.

2. Choose $T_{21} = T_{22}^{-T}(B_3^T P_0 B_1 + R_{21})$.

3. Perform the Cholesky factorization $T_{11}^T T_{11} = T_{21}^T T_{21} - B_1^T P_0 B_1 - R_{11}$.

One of the key steps in deriving this result from (38) was using matrix variable elimination to eliminate the controller parameters from the optimization problem. This would not have been possible if we had used the

20

$\mathcal{H}_2$ norm characterization (7) instead of the characterization (8).

It was also shown [4] that if $J_{fi,\epsilon_0} \neq \infty$, then $J_{fi,\epsilon} \neq \infty$ for all $\epsilon \in (0, \epsilon_0)$. Note that this corresponds to $J_{fi,\epsilon} \neq \infty$ for all $\epsilon^{-1} > \epsilon_0^{-1}$. Unlike the previous section, there is no Riccati equation result that allows us to check whether or not there exists a value of ϵ such that $J_{fi,\epsilon} \neq \infty$. This is the case because the existence of such a value of ϵ is equivalent to the solvability of a full information $\mathcal{H}_\infty$ control problem which might not be solvable via a Riccati equation. Despite this, if (34) is feasible, we can always find values of $\epsilon > 0$ for which the inner optimization problem in (38) is feasible simply by decreasing $\epsilon > 0$ until $J_{fi,\epsilon} \neq \infty$.

With this in mind, we would like to know how $J_{fi,\epsilon}$ varies as ϵ varies. Using the same reasoning as in the previous section, we see that $J_{fi,\epsilon}$ is an analytic function of ϵ. We will therefore find the global optimal value of $J_{fi,\epsilon}$ by finding a value of ϵ such that $(d/d\epsilon)(J_{fi,\epsilon}) = 0$. Implicitly differentiating the DARE $\mathcal{R}_\phi(P_0) = P_0$ and differentiating the expression for $\mathcal{R}_\psi(P_0)$ with respect to ϵ yields

$$
\begin{aligned}
\frac{d}{d\epsilon}(P_0) &= \left(A + \begin{bmatrix} B_1 & B_3 \end{bmatrix} \mathcal{K}_\phi(P_0)\right)^T \frac{d}{d\epsilon}(P_0) \left(A + \begin{bmatrix} B_1 & B_3 \end{bmatrix} \mathcal{K}_\phi(P_0)\right) \\
&\quad + \left(C_2 + \begin{bmatrix} D_{21} & D_{23} \end{bmatrix} \mathcal{K}_\phi(P_0)\right)^T \left(C_2 + \begin{bmatrix} D_{21} & D_{23} \end{bmatrix} \mathcal{K}_\phi(P_0)\right) \quad \text{(43a)}
\end{aligned}
$$

$$
\begin{aligned}
\frac{d}{d\epsilon}(\mathcal{R}_\psi(P_0)) &= \left(B_2 + \begin{bmatrix} B_1 & B_3 \end{bmatrix} \mathcal{K}_\psi(P_0)\right)^T \frac{d}{d\epsilon}(P_0) \left(B_2 + \begin{bmatrix} B_1 & B_3 \end{bmatrix} \mathcal{K}_\psi(P_0)\right) \\
&\quad + \left(D_{22} + \begin{bmatrix} D_{21} & D_{23} \end{bmatrix} \mathcal{K}_\psi(P_0)\right)^T \left(D_{22} + \begin{bmatrix} D_{21} & D_{23} \end{bmatrix} \mathcal{K}_\psi(P_0)\right). \quad \text{(43b)}
\end{aligned}
$$

The first of these equations is a discrete Lyapunov equation for $(d/d\epsilon)(P_0)$. Since $A + [B_1 \ B_3]\mathcal{K}_\phi(P_0)$ is stable (by the definition of a stabilizing solution of a DARE), we see that there exists upper triangular U such that $U^T U = (d/d\epsilon)(\epsilon P_0)$ and we can directly solve for U using the `dlyapchol` function in MATLAB. Using this, we express

$$
\frac{d}{d\epsilon}(J_{fi,\epsilon}) = -\epsilon^{-2}\text{tr}\{\mathcal{R}_\psi(P_0)\} + \epsilon^{-1}\text{tr}\left\{\frac{d}{d\epsilon}(\mathcal{R}_\psi(P_0))\right\} \quad \text{(44)}
$$

which implies that

$$
\begin{aligned}
\frac{d}{d\epsilon}(J_{fi,\epsilon}) &= \epsilon^{-1}\left(\left\|U\left(B_2 + \begin{bmatrix} B_1 & B_3 \end{bmatrix} \mathcal{K}_\phi(P_0)\right)\right\|_F^2 \right. \\
&\quad \left. + \left\|D_{22} + \begin{bmatrix} D_{21} & D_{23} \end{bmatrix} \mathcal{K}_\phi(P_0)\right\|_F^2 - J_{fi,\epsilon}\right) \quad \text{(45)}
\end{aligned}
$$

The value and derivative of $J_{fi,\epsilon}$ is also useful for generating a lower bound on the optimal value of (38). Consider Fig. 13, which shows a representative graph of $J_{fi,\epsilon}$ in which ϵ_0 is known to be a lower bound on the minimizing value of ϵ. By convexity, if ϵ_1 is known to be an upper bound on the minimizing value of ϵ,
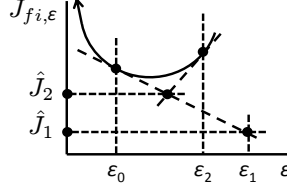
Figure 13: Illustration of lower bound computation in optimal full information $\mathcal{H}_2$ guaranteed cost control

the value and derivative of $J_{fi,\epsilon}$ at ϵ_0 gives us the lower bound $\hat{J}_1$. If instead, the value and derivative of $J_{fi,\epsilon}$ at ϵ_0 and ϵ_2 is known, we have the lower bound $\hat{J}_2$. These lower bounds are respectively given by

$$\hat{J}_1 = J_{fi,\epsilon_0} + \bar{m}_0(\epsilon_1 - \epsilon_2) \tag{46a}$$

$$\hat{J}_2 = \frac{\bar{m}_2[\bar{m}_0(\epsilon_2 - \epsilon_0) - (J_{fi,\epsilon_2} - J_{fi,\epsilon_0})]}{\bar{m}_2 - \bar{m}_0} + J_{fi,\epsilon_2} \tag{46b}$$

where J_{fi,ϵ_i} is interpreted as $J_{fi,\epsilon}$ evaluated at $\epsilon = \epsilon_i$ and $\bar{m}_i$ is $(d/d\epsilon)(J_{fi,\epsilon})$ evaluated at $\epsilon = \epsilon_i$. It should be noted that the second of these lower bounds is less conservative when it is applicable.

With these results in place, we can easily solve (38) using the following methodology:

1. **Find Initial Interval:** Choose $\alpha > 1$. Check if $J_{fi,\epsilon} \neq \infty$ and $(d/d\epsilon)(J_{fi,\epsilon}) < 0$ when $\epsilon = 1$. If so, start from $k = 1$ and increment k until either of these conditions fail to be met when $\epsilon = \alpha^k$. Denoting the corresponding value of ϵ as ϵ_u, there exists an optimal value of ϵ in the interval $(\alpha^{-1}\epsilon_u, \epsilon_u)$.

   If instead either $J_{fi,\epsilon} = \infty$ or $(d/d\epsilon)(J_{fi,\epsilon}) > 0$ when $\epsilon = 1$, start from $k = 1$ and increment k until $J_{fi,\epsilon} \neq \infty$ and $(d/d\epsilon)(J_{fi,\epsilon}) < 0$ when $\epsilon = \alpha^{-k}$. Denoting the corresponding value of ϵ as ϵ_l, there exists an optimal value of ϵ in the interval $(\epsilon_l, \alpha\epsilon_l)$.

2. **Bisection:** Solve the equation $(d/d\epsilon)(J_{fi,\epsilon}) = 0$ over ϵ using bisection. Use (45) for evaluating $(d/d\epsilon)(J_{fi,\epsilon})$. Whenever, for a particular value of ϵ, the DARE $\mathcal{R}_\phi(P) = P$ does not have a stabilizing solution $P_0 \succeq 0$ such that the factorization (41) exists for invertible T_{11} and T_{22}, this value of ϵ is an upper bound on the optimal value of ϵ.

3. **Controller Construction:** For the value of ϵ which yielded the smallest cost, reconstruct the corresponding controller using (42).

In our implementation, we use $\alpha = 100$ and, in the bisection step, we use the geometric mean instead of the arithmetic mean. We use two stopping criteria in our implementation. If we define the relative error as $\nu_{fi} := 1 - \underline{J}_{fi}/J_{fi,\epsilon}$ where $\underline{J}_{fi}$ is the lower bound computed by (46), we terminate the algorithm when either $\nu_{fi} < 10^{-10}$ or 30 iterations have been executed in steps 1–2.

22

Table 5: Analysis of closed-loop HDD performance using three approaches

Approach	Optimization Time (s)	$\mathcal{H}_2$ Cost	Guaranteed	Optimal ϵ
DARE	0.37	5.9604	1
SeDuMi	4.4616	5.938	1.0005
mincx	27.5342	5.9604	1

4.3   Application to Hard Disk Drives

So far in this section, we have developed two methodologies for designing an optimal full information controller in terms of its $\mathcal{H}_2$ guaranteed cost—one based on the solution of a SDP and another based on nonlinear convex optimization involving Riccati equation solutions.

Although we would like to apply these methodologies to the model G_H introduced in Sect. 2, it is not in the form of a full information control problem. However, we can create a full information control problem by replacing the measurements generated by the model, y, by the vector $[x^T\ d^T\ w_a^T\ w_r^T\ w_n^T]^T$ where x is the state of G_H. The model was not balanced after redefining the measurement vector.

We used three approaches to find optimal full information $\mathcal{H}_2$ guaranteed cost controllers for this system: solving the SDP (34) using the mincx command, solving (34) using SeDuMi and YALMIP, and solving (38) using the methodology at the end of Sect. 4.2. We will refer to the latter of these approaches as the DARE approach. Using these three approaches on the model of G_H with the redefined measurement vector yielded the results listed in Table 5. Although the DARE approach and the mincx approach yielded similar accuracy, the SeDuMi approach seemed to yield better accuracy. However, analyzing the closed-loop systems using the DARE approach in Sect. 3.2 showed that the actual $\mathcal{H}_2$ guaranteed cost performance achieved by controller designed using the SeDuMi approach was only 5.9671, whereas the other two controllers achieved the costs stated in Table 5. Thus, for this system, SeDuMi actually had the worst numerical accuracy of the three approaches. In terms of efficiency, the DARE approach was more than 10 times faster than the other two approaches. The difference in computation time is less dramatic than the difference in Sect. 3.3 because the closed-loop systems here have 19 states whereas the system analyzed in Sect. 3.3 had 38 states.

We now look more closely at the DARE approach to this problem. In particular, we are interested in the values of $J_{fi,\epsilon}$ and $(d/d\epsilon)(J_{fi,\epsilon})$ as functions of ϵ. Figure 14 shows a plot of these two quantities for 50 linearly spaced points in the interval $[0, 1.2]$ along with an estimate of $(d/d\epsilon)(J_{fi,\epsilon})$ obtained by applying the central difference approximation to $J_{fi,\epsilon}$. As we would expect, the curves are smooth, $(d/d\epsilon)(J_{fi,\epsilon})$ is monotonic non-decreasing, and the computed values of $(d/d\epsilon)(J_{fi,\epsilon})$ agree with the central difference approximations. Also, for this particular example, $J_{fi,\epsilon}$ is monotonic decreasing over the chosen values of ϵ.
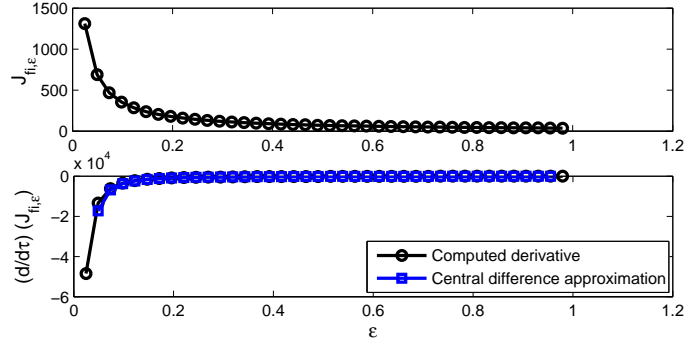
Figure 14: $J_{fi,\epsilon}$, the computed value of $(d/d\epsilon)(J_{fi,\epsilon})$, and the central difference approximation to $(d/d\epsilon)(J_{fi,\epsilon})$

Table 6: Analysis of closed-loop HDD performance for each closed-loop signal

Signal	$\mathcal{H}_2$ Guaranteed Cost
y_h	5.9551nm
u_v	0.2439V
u_p	0.0635V

The $\mathcal{H}_2$ guaranteed costs computed so far reflect a combination of the "sizes" of the signals y_h, u_v, and u_p. However, it is more meaningful to look at the "sizes" of these three signals separately. As in Sect. 3.3, we remove the outputs we are not interested in and compute the relevant $\mathcal{H}_2$ guaranteed costs associated with each output signal. Doing this for the closed-loop system designed using the DARE approach yields the $\mathcal{H}_2$ guaranteed cost given in Table 6. Thus, we see that the control effort is rather small for this controller. This suggests that we should deemphasize the control effort in the cost function in order to design controllers which achieve a higher level of performance.

5   Output Feedback H2 Guaranteed Cost Control

In this section, we consider the optimal output feedback $\mathcal{H}_2$ guaranteed cost control problem. We first present a non-convex optimization problem for determining an optimal controller and a solution heuristic which is based on the solution of SDPs. We then give an algorithm which exploits Riccati equation structure to give a more computationally efficient heuristic for finding an optimal controller. For the sake of brevity and clarity of presentation, we do not give full proofs here; these will be presented in future papers.

5.1 Sequential Semi-Definite Programming Approach

We now consider an optimal $\mathcal{H}_2$ guaranteed cost control problem of the form shown in Fig. 15a on p. 31 in which G has the known state-space realization

$$
G \sim \left[
\begin{array}{c|ccc}
A & B_1 & B_2 & B_3 \\
\hline
C_1 & D_{11} & D_{12} & D_{13} \\
C_2 & D_{21} & D_{22} & D_{23} \\
C_3 & D_{31} & D_{32} & 0
\end{array}
\right] .
\tag{47}
$$

Note that we are choosing many of the state-space entries to be the same as in the previous section. The only difference is the choice of information that is available to the controller. In this context, we are interested in finding a controller K which achieves the best possible $\mathcal{H}_2$ guaranteed cost using only the measurements y. We will refer to this as the output feedback control problem.

Using techniques similar to the one used in [4], it can be shown that, given any state-space controller, it is always possible to construct a state-space controller with the same number of states as G that achieves the same $\mathcal{H}_2$ guaranteed cost. This allows us, without any loss of closed-loop performance, to consider only state-space controllers of the form

$$
K \sim \left[
\begin{array}{c|c}
A_c & B_c \\
\hline
C_c & D_c
\end{array}
\right]
\tag{48}
$$

where A_c has the same dimensions as A.

5.1.1 Coordinate Descent Approach

We are interested in solving the optimization problem

$$
\inf_{\tau > 0, K} J_\tau(\mathcal{F}_l(G, K))
\tag{49}
$$

where K has the realization (48). Applying the Lyapunov shaping paradigm [15] to the characterization (15) for the system $\mathcal{F}_l(G, K)$ yields the optimization problem

$$
\inf_{\tau, X, Y, W, \hat{V}_1, \hat{V}_2, \hat{A}, \hat{B}, \hat{C}, \hat{D}} \operatorname{tr}\{W\} \quad \text{s.t.} \quad \check{\mathcal{M}}(\tau, X, Y, W, \hat{V}_1, \hat{V}_2, \hat{A}, \hat{B}, \hat{C}, \hat{D}) \succ 0
\tag{50}
$$

25

where

$$
\check{\mathcal{M}} \ := \ \begin{bmatrix}
X & \bullet & \bullet & \bullet & \bullet & \bullet & \bullet & \bullet \\
I & Y & \bullet & \bullet & \bullet & \bullet & \bullet & \bullet \\
0 & 0 & \tau I & \bullet & \bullet & \bullet & \bullet & \bullet \\
\hat{V}_1 & \hat{V}_2 & 0 & W & \bullet & \bullet & \bullet & \bullet \\
\check{M}_{11} & \check{M}_{12} & \check{M}_{13} & \check{M}_{14} & X & \bullet & \bullet & \bullet \\
\check{M}_{21} & \check{M}_{22} & \check{M}_{23} & \check{M}_{24} & I & Y & \bullet & \bullet \\
\tau\check{M}_{31} & \tau\check{M}_{32} & \tau\check{M}_{33} & \tau\check{M}_{34} & 0 & 0 & \tau I & \bullet \\
\check{M}_{41} & \check{M}_{42} & \check{M}_{43} & \check{M}_{44} & 0 & 0 & 0 & I
\end{bmatrix}
\tag{51a}
$$

$$
\begin{bmatrix}
\check{M}_{11} & \cdots & \check{M}_{14} \\
\vdots & \ddots & \vdots \\
\check{M}_{41} & \cdots & \check{M}_{44}
\end{bmatrix}
:=
\begin{bmatrix}
AX + B_3\hat{C} & A + B_3\hat{D}C_3 & B_1 + B_3\hat{D}D_{31} & B_2 + B_3\hat{D}D_{32} \\
\hat{A} & YA + \hat{B}C_3 & YB_1 + \hat{B}D_{31} & YB_2 + \hat{B}D_{32} \\
C_1X + D_{13}\hat{C} & C_1 + D_{13}\hat{D}C_3 & D_{11} + D_{13}\hat{D}D_{31} & D_{12} + D_{13}\hat{D}D_{32} \\
C_2X + D_{23}\hat{C} & C_2 + D_{23}\hat{D}C_3 & D_{21} + D_{23}\hat{D}D_{31} & D_{22} + D_{23}\hat{D}D_{32}
\end{bmatrix}.
\tag{51b}
$$

For any feasible $\tau, X, Y, W, \hat{V}_1, \hat{V}_2, \hat{A}, \hat{B}, \hat{C}, \hat{D}$, a controller that achieves the squared $\mathcal{H}_2$ guaranteed cost $\mathrm{tr}\{W\}$ (or better) is given by

$$
K \sim \left[
\begin{array}{c|c}
N^{-1}[\hat{A} - YAX - \hat{B}C_3X - YB_3(\hat{C} - \hat{D}C_3X)]M^{-T} & N^{-1}(\hat{B} - YB_3\hat{D}) \\
\hline
(\hat{C} - \hat{D}C_3X)M^{-T} & \hat{D}
\end{array}
\right]
\tag{52}
$$

where M and N are chosen so that

$$
MN^T = I - XY .
\tag{53}
$$

Although we use the QR decomposition to factorize $I - XY$ in our implementation, a pivoted LU decomposition would be equally suitable.

The optimization (50) is a nonconvex optimization because the matrix inequality is nonlinear in the optimization parameters; the products τX, $\tau\hat{C}$ and $\tau\hat{D}$ appear in the matrix inequality. Thus, the matrix inequality is a bilinear matrix inequality (BMI) and the optimization (50) is a BMI optimization problem. If the value of τ is fixed or the values of X, $\hat{C}$, and $\hat{D}$ are fixed, then the BMI becomes an LMI. In either of these cases, if the strict inequalities in (50) are relaxed to a non-strict inequalities, the optimization becomes a SDP. Thus, for a given initial guess for τ, a reasonable heuristic for solving (50) is to alternate between solving (50) for fixed τ and solving (50) for fixed X, $\hat{C}$, and $\hat{D}$.

There are two challenges in using this approach. The first difficultly we encounter is the difficulty of selecting the initial value of τ; since BMI optimization problems are non-convex, the selection of a "good" initial iterate is especially critical. The second difficulty that we encounter is in reconstructing the controller using (52). In particular, since the controller reconstruction depends on both M^{-1} and N^{-1}, we see that the controller reconstruction will be ill-conditioned if $I - XY$ is ill-conditioned with respect to inversion. We will show in the next two sections that it is possible to deal with both of these problem using semi-definite programming.

5.1.2 Initial Controller Design

We now examine the problem of finding an initial value of τ. To deal with this problem, we follow the approach used in [10] in which the solution of two SDPs yield initial values of all optimization parameters. Since we are only interested in the initial value of τ, we will not explicitly construct initial values for the remaining optimization parameters in this paper.

The first convex optimization is a state feedback control design. This is done by relaxing (34) to an SDP, and then solving it with the additional constraints that $\hat{K}_d = 0$ and $K_w = 0$. This yields a state feedback control law $u = K_x x$, where K_x is a static gain and x is the state variable of G.

In the second convex optimization, we first restrict the class of controllers to ones which have $C_c = K_x$ and $D_c = 0$. If the state variable of the controller is interpreted as an estimate of the state of G, this restriction can be interpreted as imposing a "separation structure" on the controller. We then form a realization of $\mathcal{F}_l(G, K)$ whose state is given by $[x^T (x - x_c)^T]^T$ where x_c is the state variable of K. Using the characterization (15) for this realization with the restriction $P = \text{diag}[\tilde{X}, \tilde{Y}]$ and the change of variables

$$\left[\begin{array}{cc} \tilde{A} & \tilde{B} \end{array} \right] := \tilde{Y} \left[\begin{array}{cc} A_c & B_c \end{array} \right] \tag{54}$$

yields the optimization problem

$$
\inf_{\tau,\tilde{X},\tilde{Y},W,V_1,V_2,\tilde{A},\tilde{B}} \mathrm{tr}\{W\} \quad \text{s.t.} \quad
\begin{bmatrix}
\tilde{X} & \bullet & \bullet & \bullet & \bullet & \bullet & \bullet & \bullet \\
0 & \tilde{Y} & \bullet & \bullet & \bullet & \bullet & \bullet & \bullet \\
0 & 0 & \tau I & \bullet & \bullet & \bullet & \bullet & \bullet \\
V_1 & V_2 & 0 & W & \bullet & \bullet & \bullet & \bullet \\
\tilde{M}_{11} & \tilde{M}_{12} & \tilde{M}_{13} & \tilde{M}_{14} & \tilde{X} & \bullet & \bullet & \bullet \\
\tilde{M}_{21} & \tilde{M}_{22} & \tilde{M}_{23} & \tilde{M}_{24} & 0 & \tilde{Y} & \bullet & \bullet \\
\tilde{M}_{31} & \tilde{M}_{32} & \tilde{M}_{33} & \tilde{M}_{34} & 0 & 0 & \tau I & \bullet \\
\tilde{M}_{41} & \tilde{M}_{42} & \tilde{M}_{43} & \tilde{M}_{44} & 0 & 0 & 0 & I
\end{bmatrix} \succ 0
\tag{55}
$$

where

$$
\begin{bmatrix}
\tilde{M}_{11} & \cdots & \tilde{M}_{14} \\
\vdots & \ddots & \vdots \\
\tilde{M}_{41} & \cdots & \tilde{M}_{44}
\end{bmatrix} :=
\begin{bmatrix}
\tilde{X}A_{cl} & -\tilde{X}B_3 K_x & \tilde{X}B_1 & \tilde{X}B_2 \\
\tilde{Y}A_{cl} - \tilde{A} - \tilde{B}C_3 & \tilde{A} - \tilde{Y}B_3 K_x & \tilde{Y}B_1 - \tilde{B}D_{31} & \tilde{Y}B_2 - \tilde{B}D_{32} \\
\tau(C_1 + D_{13}K_x) & -\tau D_{13}K_x & \tau D_{11} & \tau D_{12} \\
C_2 + D_{23}K_x & -D_{23}K_x & D_{21} & D_{22}
\end{bmatrix}
\tag{56}
$$

and $A_{cl} := A + B_3 K_x$. Although it is not used by our algorithm developed here, it is worth mentioning that, for any feasible $\tau, \tilde{X}, \tilde{Y}, W, V_1, V_2, \tilde{A}, \tilde{B}$, a controller which achieves the squared $\mathcal{H}_2$ guaranteed cost $\mathrm{tr}\{W\}$ or better is given by

$$
K \sim \left[\begin{array}{c|c}
\tilde{Y}^{-1}\tilde{A} & \tilde{Y}^{-1}\tilde{B} \\
\hline
K_x & 0
\end{array}\right].
\tag{57}
$$

If the strict inequalities in (55) are relaxed to a non-strict inequalities, the optimization becomes a SDP. The value of τ which results from solving this optimization problem is a suitable initial value of τ for the BMI optimization problem (50).

5.1.3 Conditioning of the Controller Reconstruction Step

As mentioned in Sect. 5.1.1, we would like to make the matrix $I - XY$ well-conditioned with respect to inversion. Define

$$
S := \begin{bmatrix} X & I \\ I & Y \end{bmatrix}.
\tag{58}
$$

Since $S \succ 0$ for any feasible iterate of (50), we see by Schur complements that $Y \succ 0$ and $X - Y^{-1} \succ 0$ for any feasible iterate of (50). In particular, Y and $X - Y^{-1}$ are invertible. Exploiting the invertibility of these

matrices yields

$$S^{-1} = \begin{bmatrix} (X - Y^{-1})^{-1} & (I - YX)^{-1} \\ (I - XY)^{-1} & Y^{-1} + Y^{-1}(X - Y^{-1})^{-1}Y^{-1} \end{bmatrix}. \tag{59}$$

Since $(I - XY)^{-1}$ explicitly appears in the expression for S^{-1}, we see that if S is easy to invert then $I - XY$ must also be easy to invert. Since S is a positive definite matrix for any feasible iterate of (50), we would therefore like to make the ratio of its largest eigenvalue to its smallest eigenvalue (i.e. its condition number) as small as possible.

Since the condition number of $S \succ 0$ is less than κ if and only if there exists $t > 0$ such that $I \prec tS \prec \kappa I$, we see that a reasonable way to improve the conditioning of the controller reconstruction is to solve

$$\inf_{t,\kappa,tX,tY,tW,t\hat{V}_1,t\hat{V}_2,t\hat{A},t\hat{B},t\hat{C},t\hat{D}} \kappa \quad \text{s.t.} \quad t\check{\mathcal{M}} \succ 0, \quad I \prec tS \prec \kappa I, \quad \text{tr}\{tW\} < t\gamma \tag{60}$$

where γ is some acceptable level of $\mathcal{H}_2$ guaranteed cost performance for the closed-loop system. Note that we have fixed the value of τ and the level of $\mathcal{H}_2$ guaranteed cost performance in this optimization. Also note that $t\check{\mathcal{M}} \succ 0$ implies that $t > 0$. Thus, this optimization problem minimizes the condition number of S subject to a constraint on the closed-loop $\mathcal{H}_2$ guaranteed cost and a fixed value of τ.

When the strict inequalities in (60) are relaxed to non-strict inequalities, it becomes an SDP in the variables t, κ, tX, tY, tW, $t\hat{V}_1$, $t\hat{V}_2$, $t\hat{A}$, $t\hat{B}$, $t\hat{C}$, and $t\hat{D}$. Thus, improving the conditioning of the the controller reconstruction process for a fixed value of τ and a fixed closed-loop $\mathcal{H}_2$ guaranteed cost can be solved using this SDP.

5.1.4   Solution Methodology

With the results of the previous sections in place, a reasonable methodology for trying to solve (49) is:

1. **Find Initial Value of τ**

   (a) **State Feedback Controller Design:** Solve (34) with the additional constraints that $\hat{K}_d = 0$ and $K_w = 0$ using an SDP solver. From the resulting set of optimization parameter values, reconstruct the state feedback gain $K_x := \hat{K}_x \hat{P}^{-1}$.

   (b) **"Separation Principle" Controller Design:** Solve (55) using an SDP solver.

2. **Controller Design**

   (a) **Controller Design (Fixed τ):** Fix τ to be the value obtained in the previous optimization. Solve (50) using an SDP solver.

(b) **Controller Design (Fixed $X, \hat{C}, \hat{D}$):** Fix X, $\hat{C}$, and $\hat{D}$ to be the values obtained in the previous optimization. Solve (50) using an SDP solver. If the stopping criteria have not been met (see below), return to step 2a.

3. **Conditioning:** Choose a value of $\beta > 0$. Fix τ to be the value which yielded the smallest cost γ_0 in the preceding optimizations[1] and fix γ to be $(1+\beta)\gamma_0$. Solve (60) using an SDP solver.

4. **Controller Reconstruction:** Reconstruct the controller using (52).

In our implementation of the algorithm, although we choose the default $\beta = 0.05$, we allow this to be specified by the user. This allows the user to trade off closed-loop performance versus conditioning in the controller reconstruction step. We use two stopping criteria in step 2. If 6 total optimizations have been performed in step 2 or if the cost has decreased less than 1% in the last two optimizations, we exit step 2 and move on to step 3.

5.2 Riccati Equation and Semi-Definite Programming Approach

In this section, we consider the output feedback control problem when the regularity conditions of Sect. 4.2 hold. For now, we fix $\tau > 0$ and consider the problem of optimizing $J_\tau(\mathcal{F}_l(G, K))$. The approach we follow is similar to the approach taken in solving the discrete-time $\mathcal{H}_\infty$ control problem [9]. However, since $\mathcal{H}_2$ guaranteed cost control does not have a frequency-domain interpretation, we directly manipulate Riccati equations to establish the relevant results.

If there exists an output feedback controller which achieves a finite value of $J_\tau(\mathcal{F}_l(G, K))$, then there exists a full information controller which achieves finite cost, i.e. $J_{fi,\epsilon} \neq \infty$ for $\epsilon = \tau^{-1}$. Thus, we begin by solving the full information problem for $\epsilon = \tau^{-1}$. We will denote the stabilizing solution of the DARE $\mathcal{R}_\phi(P) = P$ (which is assumed to satisfy the relevant properties) as P_0. In addition to the notation from Sect. 4.2, we also define the notation

$$
\begin{align}
K_{dx} &:= T_{11}^{-1}T_{11}^{-T}[B_1^T P_0 A + D_{11}^T C_1 + \epsilon D_{21}^T C_2 + (B_3^T P_0 B_1 + R_{21})^T K_x] \tag{61a}\\
K_{dw} &:= T_{11}^{-1}T_{11}^{-T}[B_1^T P_0 B_2 + D_{11}^T D_{12} + \epsilon D_{21}^T D_{22} + (B_3^T P_0 B_1 + R_{21})^T K_w] \tag{61b}\\
\bar{K}_x &:= K_x + K_d K_{dx} \tag{61c}\\
\bar{K}_w &:= K_w + K_d K_{dw} \, . \tag{61d}
\end{align}
$$

---

[1] Although the value of the optimization problem should decrease every time steps 2a or 2b is executed, numerical inaccuracies might cause this not to be the case.
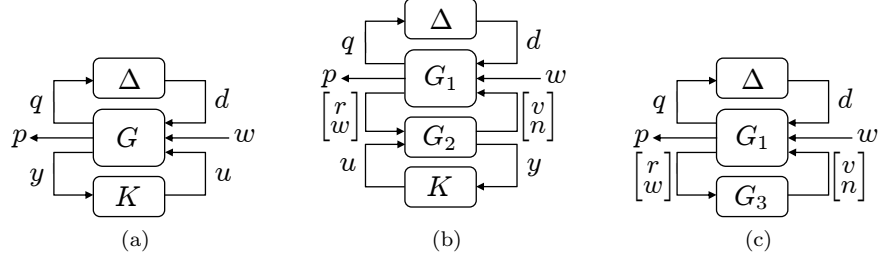
Figure 15: Three equivalent block diagrams for output feedback $\mathcal{H}_2$ guaranteed cost control structure

In this notation, it can be shown that

$$\mathcal{K}_\phi(P_0) = \begin{bmatrix} K_{dx} \\ \bar{K}_x \end{bmatrix}.$$

(62)

5.2.1 Reduction to Output Estimation Problem

We now consider Fig. 15b where the state-space realizations of G_1 and G_2 are respectively given by

$$G_1 \sim \left[\begin{array}{c|cccc} A + B_3 K_x & B_1 + B_3 K_d & B_2 + B_3 K_w & B_3 T_{22}^{-1} & 0 \\ \hline C_1 + D_{13} K_x & D_{11} + D_{13} K_d & D_{12} + D_{13} K_w & D_{13} T_{22}^{-1} & 0 \\ C_2 + D_{23} K_x & D_{21} + D_{23} K_d & D_{22} + D_{23} K_w & D_{23} T_{22}^{-1} & 0 \\ -T_{11} K_{dx} & T_{11} & -T_{11} K_{dw} & 0 & 0 \\ 0 & 0 & I & 0 & 0 \end{array}\right]$$

(63a)

$$G_2 \sim \left[\begin{array}{c|ccc} A + B_1 K_{dx} & B_1 T_{11}^{-1} & B_2 + B_1 K_{dw} & B_3 \\ \hline -T_{22} \bar{K}_x & -T_{22} K_d T_{11}^{-1} & -T_{22} \bar{K}_w & T_{22} \\ 0 & 0 & 0 & 0 \\ C_3 + D_{31} K_{dx} & D_{31} T_{11}^{-1} & D_{32} + D_{31} K_{dw} & 0 \end{array}\right].$$

(63b)

Note that, with these definitions of G_1 and G_2, the signal n is zero. Although n does not play a role in the dynamics of the system, we will see later in this section that it serves a structural role. Using the fact that $A + [B_1 \ B_3]\mathcal{K}_\phi(P_0)$ is Schur (by the definition of a stabilizing DARE solution), it can be shown that combining G_1 and G_2 into a single block yields the block diagram in Fig. 15a. If we instead combine G_2 and K into a single block, G_3, it yields the block diagram in Fig. 15c. Thus, the three block diagrams in Fig. 15 are equivalent.

Now suppose that G_3 has the realization

$$G_3 \sim \left[\begin{array}{c|cc} \tilde{A} & \tilde{B}_1 & \tilde{B}_2 \\ \hline \tilde{C} & \tilde{D}_1 & \tilde{D}_2 \\ 0 & 0 & 0 \end{array} \right] . \tag{64}$$

Note that although we are utilizing the fact that $n = 0$, we are not explicitly expoiting any other structure of G_3. With this in place, we are interested in evaluating $J_\tau(\mathcal{F}_l(G_1, G_3))$. It can be shown that

$$J_\tau(\mathcal{F}_l(G_1, G_3)) = J_{fi,\epsilon} + \epsilon^{-1} J_1(G_3) \tag{65}$$

where $J_1(G_3)$ is interpreted as $J_\tau(G_3)$ at $\tau = 1$. Using the techniques of Sect. 3.2, $J_1(G_3) = \text{tr}\{\mathcal{R}_{\tilde{\psi}}(\tilde{P}_0)\}$ where $\tilde{P}_0$ is the stabilizing solution of the DARE $\mathcal{R}_{\tilde{\phi}}(P) = P$ such that $\tilde{B}_1^T \tilde{P}_0 \tilde{B}_1 + \tilde{D}_1^T \tilde{D}_1 - I \prec 0$ where

$$\tilde{\phi} \quad := \quad (\tilde{A}, \ \tilde{B}_1, \ \tilde{C}^T \tilde{C}, \ \tilde{D}_1^T \tilde{D}_1 - I, \ \tilde{C}^T \tilde{D}_1) \tag{66a}$$

$$\tilde{\psi} \quad := \quad (\tilde{B}_2, \ \tilde{B}_1, \ \tilde{D}_2^T \tilde{D}_2, \ \tilde{D}_1^T \tilde{D}_1 - I, \ \tilde{D}_2^T \tilde{D}_1) . \tag{66b}$$

It should be noted that (65) could only be written in such a compact form due to the placeholder signal n; without that placeholder, G_3 would only have one output and the expression $J_\tau(G_3)$ would not be well-defined.

The proof of (65) proceeds along the following lines. First, find a realization of $\mathcal{F}_l(G_1, G_3)$ with $[x_1^T \ x_3^T]^T$ as the state where x_1 and x_3 are respectively the states of G_1 and G_3 and then apply the techniques of Sect. 3.2. This yields that $J_\tau(\mathcal{F}_l(G_1, G_3)) = \text{tr}\{\mathcal{R}_{\check{\psi}}(\check{P}_0)\}$ where $\check{P}_0$ is the stabilizing solution of the DARE $\mathcal{R}_{\check{\phi}}(P) = P$ such that the relevant matrix is negative definite. (The exact expressions of the relevant quantities are omitted for brevity.) Using the matrix pencil method for analyzing DAREs [11], it can be shown that $\check{P}_0$ has the form $\text{diag}[P_0, \epsilon^{-1} P_{22}]$ for some matrix P_{22}. Using this expression, the DARE $\mathcal{R}_{\check{\phi}}(P) = P$ can be written

$$\left[\begin{array}{cc} P_0 & 0 \\ 0 & \epsilon^{-1} P_{22} \end{array} \right] = \left[\begin{array}{cc} P_0 & 0 \\ 0 & \epsilon^{-1} \mathcal{R}_{\tilde{\phi}}(P_{22}) \end{array} \right] . \tag{67}$$

Thus, with a little more algebra, it can be shown that the existence of the stabilizing DARE solution such that the relevant matrix is negative definite is equivalent to the existence of $\tilde{P}_0$ with the relevant properties. Moreover, $\check{P}_0 = \text{diag}[P_0, \epsilon^{-1} \tilde{P}_0]$. Plugging this into the expression for $\mathcal{R}_{\check{\psi}}(\check{P}_0)$ yields after some algebra that $\mathcal{R}_{\check{\psi}}(\check{P}_0) = \epsilon^{-1} \mathcal{R}_\psi(P_0) + \epsilon^{-1} \mathcal{R}_{\tilde{\psi}}(\tilde{P}_0)$. This immediately gives (65).
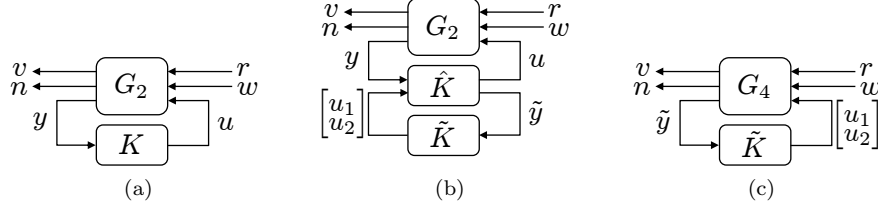
Figure 16: LFT representation of $\mathcal{H}_2$ guaranteed cost control structure

Using (65), we see that the optimization problem we are interested in solving is

$$
\begin{aligned}
\inf_K J_\tau(\mathcal{F}_l(G, K)) &= \inf_K J_\tau(\mathcal{F}_l(G_1, \mathcal{F}_l(G_2, K))) = \inf_K \left\{ J_{fi,\epsilon} + \epsilon^{-1} J_1(\mathcal{F}_l(G_2, K)) \right\} \\
&= J_{fi,\epsilon} + \epsilon^{-1} \inf_K J_1(\mathcal{F}_l(G_2, K)) .
\end{aligned}
\tag{68}
$$

The remaining optimal control problem

$$
\inf_K J_1(\mathcal{F}_l(G_2, K))
\tag{69}
$$

is analogous to the output estimation problem in the $\mathcal{H}_\infty$ literature.

5.2.2 Reduction to Full Control Problem

For $\mathcal{H}_\infty$ control, the output estimation problem is solved by applying duality—transposing the closed-loop system transfer function matrix—to transform the problem into a disturbance feedforward problem, reducing this to a full information control problem, then applying the optimal full information controller. However, in our approach, this approach does not work because there is no known duality result. Thus, we now diverge slightly from the approach taken in [9].

At this point, we restrict the class of controllers to ones which can be expressed as $K = \mathcal{F}_l(\hat{K}, \tilde{K})$ where

$$
\hat{K} \sim \left[
\begin{array}{c|ccc}
A + [B_1\ B_3]\mathcal{K}_\phi(P_0) & 0 & -I & B_3 \\
\hline
\bar{K}_x & 0 & 0 & I \\
-(C_3 + D_{31}K_{dx}) & I & 0 & 0
\end{array}
\right] .
\tag{70}
$$

For this control structure, the block diagrams in Figs. 16a and 16b are equivalent. Combining G_2 and $\hat{K}$ in Fig. 16b into a single block, G_4, yields Fig. 16c. Thus, the three block diagrams in Fig. 16 are equivalent for this control structure.

The obvious question is whether or not this control structure worsens the level of achievable performance of the closed-loop system. To answer this, we first note that, since $A + [B_1\ B_3]\mathcal{K}_\phi(P_0)$ is Schur, G_4 has the

realization

$$
G_4 \sim \left[
\begin{array}{c|ccccc}
A + B_1 K_{dx} & B_1 T_{11}^{-1} & B_2 + B_1 K_{dw} & I & 0 \\
\hline
-T_{22}\bar{K}_x & -T_{22}K_d T_{11}^{-1} & -T_{22}\bar{K}_w & 0 & T_{22} \\
0 & 0 & 0 & 0 & 0 \\
C_3 + D_{31}K_{dx} & D_{31}T_{11}^{-1} & D_{32} + D_{31}K_{dw} & 0 & 0
\end{array}
\right] .
\tag{71}
$$

Thus, we see that if we make the restriction $u_1 = B_3 u_2$ in Fig. 16c, we exactly recover the control problem shown in Fig. 16a. This means that choosing this special control structure does not affect the achievable performance of the closed-loop system. The remaining optimal control problem

$$
\inf_{\tilde{K}} J_1(\mathcal{F}_l(G_4, \tilde{K}))
\tag{72}
$$

is analogous to the full control problem in the $\mathcal{H}_\infty$ literature.

5.2.3   Solving the Full Control Problem

Using techniques similar to the one used in [4], it can be shown that, given any state-space controller for the block diagram in Fig. 16c, it is always possible to construct a static gain controller for the block diagram in Fig. 16c that achieves the same performance in terms of $J_1(\mathcal{F}_l(G_4, \tilde{K}))$. We therefore express

$$
\tilde{K} = \left[
\begin{array}{c}
L_x \\
L_v
\end{array}
\right]
\tag{73}
$$

where L_x and L_v are static gains.

It is not currently known whether or not the full control problem can be solved using Riccati equations. Therefore, to solve this problem, we will resort to the SDP approach. We first apply the change of variables $\hat{L}_x := P L_x$. Applying the characterization (15) with $\tau = 1$ to $\mathcal{F}_l(G_4, \tilde{K})$ yields, after multiplying $\bar{\mathcal{M}}$ on the right by $\Phi := \text{diag}[I, T_{11}, I, I, T_{22}, I]$ and on the left by Φ^T, the optimization problem

$$
\inf_{P,W,V,\hat{L}_x,L_v} \text{tr}\{W\} \quad \text{s.t.} \quad \left[
\begin{array}{cc}
\tilde{\mathcal{M}} & 0 \\
0 & I
\end{array}
\right] \succ 0
\tag{74}
$$

where

$$
\tilde{\mathcal{M}} := \begin{bmatrix} P & \bullet & & \bullet & \bullet & \bullet \\ 0 & T_{21}^T T_{21} - B_1^T P_0 B_1 - R_{11} & \bullet & & \bullet & \bullet \\ V & 0 & W & & \bullet & \bullet \\ P\check{A} + \hat{L}_x \check{C}_3 & PB_1 + \hat{L}_x D_{31} & & P\check{B} + \hat{L}_x \check{D}_3 & P & \bullet \\ \check{M}_1 & \check{M}_2 & & \check{M}_3 & 0 & B_3^T P_0 B_3 + R_{22} \end{bmatrix} \tag{75}
$$

and

$$
\begin{bmatrix} \check{A} & \check{B} \\ \check{C}_1 & \check{D}_1 \\ \check{C}_2 & \check{D}_2 \\ \check{C}_3 & \check{D}_3 \end{bmatrix} := \begin{bmatrix} A + B_1 K_{dx} & B_2 + B_1 K_{dw} \\ C_1 + D_{11} K_{dx} & D_{12} + D_{11} K_{dw} \\ C_2 + D_{21} K_{dx} & D_{22} + D_{21} K_{dw} \\ C_3 + D_{31} K_{dx} & D_{32} + D_{31} K_{dw} \end{bmatrix} \tag{76a}
$$

$$
\check{M}_1 := (B_3^T P_0 B_3 + R_{22})L_v \check{C}_3 + B_3^T P_0 \check{A} + D_{13}^T \check{C}_1 + \epsilon D_{23}^T \check{C}_2 \tag{76b}
$$

$$
\check{M}_2 := (B_3^T P_0 B_3 + R_{22})L_v D_{31} + B_3^T P_0 B_1 + D_{13}^T D_{11} + \epsilon D_{23}^T D_{21} \tag{76c}
$$

$$
\check{M}_3 := (B_3^T P_0 B_3 + R_{22})L_v \check{D}_3 + B_3^T P_0 \check{B} + D_{13}^T \check{D}_1 + \epsilon D_{23}^T \check{D}_2 . \tag{76d}
$$

(Recall that, in these definitions, $\epsilon = \tau^{-1}$.) Since $\mathrm{diag}[\tilde{\mathcal{M}}, I] \succ 0$ if and only if $\tilde{\mathcal{M}} \succ 0$, we see that (74) is equivalent to

$$
\inf_{P,W,V,\hat{L}_x,L_v} \mathrm{tr}\{W\} \quad \text{s.t.} \quad \tilde{\mathcal{M}} \succ 0 . \tag{77}
$$

For any feasible $P, W, V, \hat{L}_x, L_v$, a controller which achieves $J_1(\mathcal{F}_l(G_4, \tilde{K})) \leq \mathrm{tr}\{W\}$ is given by

$$
\tilde{K} = \begin{bmatrix} L_x \\ L_v \end{bmatrix} = \begin{bmatrix} P^{-1}\hat{L}_x \\ L_v \end{bmatrix} . \tag{78}
$$

Putting this result together with (65) and the structure $K = \mathcal{F}_l(\hat{K}, \tilde{K})$ yields the following result: for any feasible $P, W, V, \hat{L}_x, L_v$ of (77), an output feedback controller which achieves $J_\tau(\mathcal{F}_l(G, K)) \leq J_{fi,\epsilon} + \mathrm{tr}\{W\}$ is given by

$$
K \sim \left[\begin{array}{c|c} A + B_1 K_{dx} + B_3 \bar{K}_x + (P^{-1}\hat{L}_x - B_3 L_v)(C_3 + D_{31} K_{dx}) & P^{-1}\hat{L}_x - B_3 L_v \\ \hline L_v(C_3 + D_{31} K_{dx}) - \bar{K}_x & L_v \end{array} \right] \tag{79}
$$

If the strict inequality in (77) is relaxed to a non-strict inequality, the optimization becomes a SDP. Thus, a reasonable way to solve the output feedback control problem (for fixed τ) is to relax (77) to a SDP, solve the SDP using an appropriate solver, then reconstruct the output feedback controller using (79).

5.2.4 Solution Methodology

With the results of the previous sections in place, a reasonable methodology for trying to solve (49) is:

1. **Find Initial Value of τ**

   (a) **Full Information Controller Design:** Using the methodology of Sect. 4.2, design an optimal full information controller.

   (b) **Find Feasible Value of τ:** Choose $\alpha > 0$. For the final values determined during the last full information controller design, solve (77) using an SDP solver. If the optimization was feasible, reconstruct the corresponding output feedback controller K using (79). If the optimization was not feasible, set $\tau \leftarrow \alpha\tau$, design a full information controller for $\epsilon = \tau^{-1}$ using the methods of Sect. 4.2, and redo this step.

   (c) **Closed-Loop System Analysis (Fixed K):** Form the closed-loop system $\mathcal{F}_l(G, K)$ and analyze its $\mathcal{H}_2$ guaranteed cost performance using the methodology of Sect. 3.2.

2. **Controller Design**

   (a) **Output Feedback Controller Design (Fixed τ):** For the value of $\tau > 0$ found in the previous closed-loop system analysis step, solve (77) using an SDP solver and reconstruct the corresponding controller K using (79).

   (b) **Closed-Loop System Analysis (Fixed K):** Form the closed-loop system $\mathcal{F}_l(G, K)$ and analyze its $\mathcal{H}_2$ guaranteed cost performance using the methodology of Sect. 3.2. Return to step 2a.

In our implementation, we use $\alpha = 100$. We use two stopping criteria in this algorithm. If the number of output feedback controller optimizations (i.e. the number of times steps 1b and 2a have been executed) exceeds 30 or if $J_{of}^{[i-1]}/J_{of}^{[i]} - 1 < 10^{-4}$ where $J_{of}^{[i]}$ is the cost reported the ith time step 2b executes, we terminate the algorithm. We also terminate the algorithm if the SDP solver claims infeasibility in step 2a.

We now take a minute to explain step 1b in above methodology. By the results in Sect. 3.2, $J_\tau(\mathcal{F}_l(G, K)) \neq \infty$ implies that $J_{\bar\tau}(\mathcal{F}_l(G, K)) \neq \infty$ whenever $\bar\tau > \tau$. Therefore to find a value of τ for which there exists K satisfying $J_\tau(\mathcal{F}_l(G, K)) \neq \infty$, we should make τ increasingly large.

5.3 Application to Hard Disk Drives

So far in this section, we have developed two methodologies for designing output feedback controllers—one based on solving a sequence of SDPs and another which exploits the solution of Riccati equations to

Table 7: Closed-loop performance and cumulative optimization after each optimization step in SSDP approach

Step	$\mathcal{H}_2$ Cost	Guaranteed	Cumulative Time (s)	Optimization
1a	6.255		10.811	
1b	9.730		239.89	
2a	8.095		561.74	
2b	8.095		1188.12	
2a	8.095		1552.77	
2b	8.095		2091.08	
3	8.257		3610.92	

yield simplified SDPs. We will respectively call these approaches the SSDP approach and the DARE/SDP approach. In this section, we will design controllers for the HDD model presented in Sect. 2. As we saw in Sect. 4.3, the controllers designed for this HDD model tend to use very little control effort. In an effort to boost the PES performance of the closed-loop system (at the expense of the control effort), we will deemphasize the control effort in the cost function by applying our solution heuristics to the plant

$$\hat{G}_H := \operatorname{diag}[1, 1, 0.01, 0.01, 1] G_H . \tag{80}$$

We first applied the SSDP approach in Sect. 5.1.4 to the design of an output feedback controller for $\hat{G}_H$. Doing so yielded the results shown in Table 7, which breaks down the $\mathcal{H}_2$ guaranteed cost and the cumulative optimization time at each optimization step. The first thing to note is that the SSDP approach took just over 1 hour to design a controller for this system. The next thing to note is that, at steps 1b and 3, there are degradations in performance. However, these are both expected. At step 1a, since the designed controller has direct access to the state of $\hat{G}_H$, it is likely that the cost reported after this step is smaller than is achievable by an output feedback controller. In step 3, we allowed the cost to increase by up to 2% in order to optimize the conditioning of the controller reconstruction process; the $\mathcal{H}_2$ guaranteed cost was a design parameter rather than the objective function to be optimized.

Before performing step 3, we tried to reconstruct a controller which achieved the $\mathcal{H}_2$ guaranteed cost 8.095. However, the condition number of the matrix $I - XY$ (i.e. the ratio of its largest and smallest singular values) was 3.802×10^{22}. This resulted in large numerical inaccuracies when reconstructing the controller, which in turn resulted in an unstable closed-loop system. After performing step 3, the condition number of the matrix $I - XY$ was improved to 7.933×10^8. With the resulting values of the optimization parameters, a controller was reconstructed which achieves the $\mathcal{H}_2$ guaranteed cost 7.958 (as computed by the methodology in Sect. 3.2). Interestingly, this is 4% better than the cost reported by the solver in step 3. Figure 17 shows
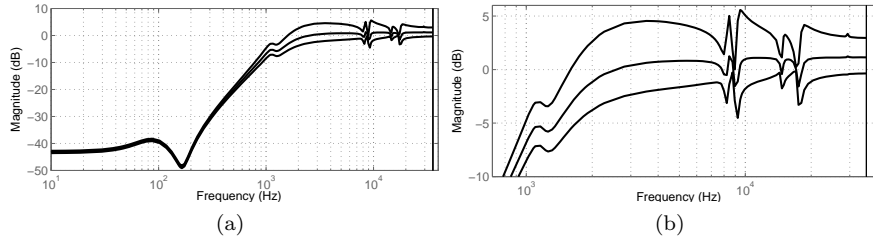
Figure 17: Bode magnitude plot of the nominal closed-loop sensitivity function from r to y_h for the controller designed using the SSDP approach along with its pointwise upper and lower bounds over all modeled uncertainty
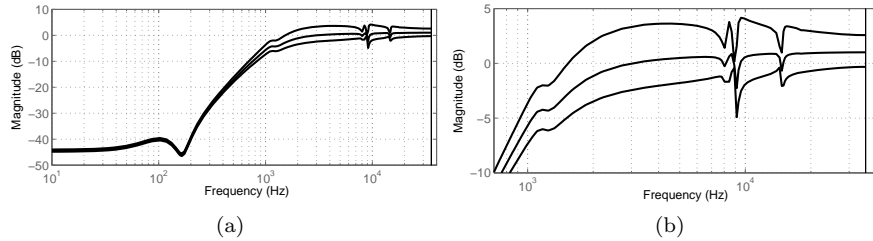
Figure 18: Bode magnitude plot of the nominal closed-loop sensitivity function from r to y_h for the controller designed using the DARE/SDP approach along with its pointwise upper and lower bounds over all modeled uncertainty

the Bode magnitude plot of nominal closed-loop sensitivity function from r to y_h along with pointwise upper and lower bounds on its Bode magnitude plot over modeled uncertainty. The nominal Bode magnitude plot has the peak value 1.25dB and the upper bound on the Bode magnitude plot has the peak value 5.57dB. Thus, even in the worst case, the Bode magnitude plot of the sensitivity function from r to y_h has a low peak.

After designing a controller using the SSDP approach, we designed a controller using the DARE/SDP approach. The algorithm took 39.03 seconds to run and reported a closed-loop $\mathcal{H}_2$ guaranteed cost of 7.747. By construction, this value of the closed-loop $\mathcal{H}_2$ guaranteed cost is exactly equal to the $\mathcal{H}_2$ guaranteed cost computed by applying the methods of Sect. 3.2 to analyze the closed-loop performance. Thus, this controller performs 2% better than the controller designed using the SSDP approach. Also note that the DARE/SDP approach was more than 90 times faster than the SSDP approach.

Figure 18 shows the Bode magnitude plot of nominal closed-loop sensitivity function from r to y_h along with pointwise upper and lower bounds on its Bode magnitude plot over modeled uncertainty. The nominal Bode magnitude plot has the peak value 1.01dB and the upper bound on the Bode magnitude plot has the peak value 4.16dB. Thus, like the closed-loop system designed using the SSDP approach, the Bode magnitude plot of the sensitivity function from r to y_h has a low "hump" in both the nominal and worst case.

Table 8: Worst-case standard deviation of closed-loop signals over 3000 random closed-loop samples with controller designed using the DARE/SDP approach

Signal	Standard Deviation
y_h	2.466nm
u_v	0.316V
u_p	0.279V

It should be noted that the $\mathcal{H}_2$ guaranteed cost performance of a system is an upper bound on the worst-case $\mathcal{H}_2$ performance of the system over all unmodeled uncertainty—not necessarily the actual worst-case performance. It is thus useful to perform a Monte Carlo analysis of the closed-loop system. Using the function `usample` in the Robust Control Toolbox, we fist chose 3000 random samples of the closed-loop system with Δ restricted to be a stable causal 3rd-order system satisfying $\|\Delta\|_\infty \leq 1$. For each of the 3000 systems, we then found the standard deviation of each of the outputs by computing the relevant $\mathcal{H}_2$ norm. The worst-case standard deviation of each signal is summarized in Table 8. We see that these results are significantly smaller than predicted by $\mathcal{H}_2$ guaranteed cost analysis of the closed-loop system.

6 Conclusion

In this chapter, we have developed two heuristics for solving the output feedback $\mathcal{H}_2$ guaranteed cost control problem. In the first method, a series of SDPs are solved to design a controller. The second method exploits the solutions of Riccati equations to simplify the output feedback control problem (for a fixed value of τ) to a full control problem, which can be solved using an SDP. These methods were applied to a track-following HDD control problem in which the HDD had a PZT-actuated suspension. It was shown that although both methods yielded controllers with a reasonable level of robust performance, the algorithm that exploited Riccati equation structure was more than 90 times faster and yielded a slightly better value of the cost function.

References

[1] Stephen Boyd, Laurent El Ghaoui, Eric Feron, and Venkataramanan Balakrishnan. *Linear Matrix Inequalities in System and Control Theory*, volume 15 of *SIAM Studies in Applied Mathematics*. Society for Industrial and Applied Mathematics, Philadelphia, 1994.

[2] Richard Conway, Sarah Felix, and Roberto Horowitz. Model reduction and parametric uncertainty

identification for robust H_2 control synthesis for dual-stage hard disk drives. *IEEE Trans. Magn.*, 43(9):3763–3768, September 2007.

[3] Richard Conway and Roberto Horowitz. Analysis of discrete-time H2 guaranteed cost performance. In *Proc. ASME Dyn. Syst. Control Conf., DSCC 2009*, number PART A, pages 427–435, 2010.

[4] Richard Conway and Roberto Horowitz. Optimal full information H2 guaranteed cost control of discrete-time systems. To appear in: Proc. ASME Dyn. Syst. Control Conf., DSCC 2010. 2010.

[5] David F. Delchamps. Analytic stabilization and the algebraic Riccati equation. In *Proc. IEEE Conf. Decis. Control*, volume 22, pages 1396–1401, December 1983.

[6] R. B. Evans, J. S. Griesbach, and W. C. Messner. Piezoelectric microactuator for dual stage control. *IEEE Trans. Magn.*, 35(2):977–982, March 1999.

[7] Toshiki Hirano, Long-Sheng Fan, Tetsuo Semba, Wen Y. Lee, John Hong, Surya Pattanaik, Patrick Webb, Wen-Han Juan, and Susanna Chan. High-bandwidth HDD tracking servo by a moving-slider micro-actuator. *IEEE Trans. Magn.*, 35(5):3670–3672, September 1999.

[8] Xinghui Huang, Ryozo Nagamune, and Roberto Horowitz. A comparison of multirate robust track-following control synthesis techniques for dual-stage and multi-sensing servo systems in hard disk drives. *IEEE Trans. Magn.*, 42(7):1896–1904, July 2006.

[9] P. A. Iglesias and K. Glover. State-space approach to discrete-time $\mathcal{H}_\infty$ control. *Int. J. Control*, 54(5):1031–1073, November 1991.

[10] S. Kanev, C. Scherer, M. Verhaegen, and B. De Schutter. Robust output-feedback controller design via local BMI optimization. *Automatica*, 40(7):1115–1127, July 2004.

[11] Peter Lancaster and Leiba Rodman. *Algebraic Riccati Equations*. Oxford Science Publications. Clarendon Press, Oxford, 1995.

[12] J. Löfberg. YALMIP : A toolbox for modeling and optimization in MATLAB. In *Proc. IEEE Int. Symp. Comput. Aided Control Syst. Des.*, pages 284–289, September 2004.

[13] Jianbin Nie and Roberto Horowitz. Design and implementation of dual-stage track-following control for hard disk drives. In *Proc. ASME Dyn. Syst. Control Conf., DSCC 2009*, number PART B, pages 1477–1484, 2010.

[14] Ian R. Petersen, Duncan C. McFarlane, and Mario A. Rotea. Optimal guaranteed cost control of discrete-time uncertain linear systems. *Int. J. Robust Nonlinear Control*, 8(8):649–657, July 1998.

[15] Carsten Scherer, Pascal Gahinet, and Mahmoud Chilali. Multiobjective output-feedback control via LMI optimization. *IEEE Trans. Autom. Control*, 42(7):896–911, July 1997.

[16] Jos F. Sturm. Using SeDuMi 1.02, a MATLAB toolbox for optimization over symmetric cones. *Optim. Methods Software*, 11:625–653, 1999.

[17] Hiroshi Toshiyoshi, Makoto Mita, and Hiroyuki Fujita. A MEMS piggyback actuator for hard-disk drives. *J. Microelectromech. Syst.*, 11(6):648–654, December 2002.

[18] L. Yu and F. Gao. Output feedback guaranteed cost control for uncertain discrete-time systems using linear matrix inequalities. *J. Optim. Theory Appl.*, 113(3):621–634, June 2002.